Title

Metal-Assisted Oxo Atom Addition to an Fe(III) Thiolate

Journal

Journal of the American Chemical Society, 139(1)

ISSN

0002-7863

Authors

Villar-Acevedo, Gloria
Lugo-Mas, Priscilla
Blakely, Maike N
et al.

Publication Date

2017-01-11

DOI

10.1021/jacs.6b03512

Peer reviewed

HHS Public Access

Author manuscript

J Am Chem Soc. Author manuscript; available in PMC 2017 January 24.

Published in final edited form as:

J Am Chem Soc. 2017 January 11; 139(1): 119–129. doi:10.1021/jacs.6b03512.

Metal-Assisted Oxo Atom Addition to an Fe(III) Thiolate

Gloria Villar-Acevedo, **Priscilla Lugo-Mas**, **Maike N. Blakely**, **Julian A. Rees**, **Abbie S. Ganas**, **Erin M. Hanada**, **Werner Kaminsky**[§], and **Julie A Kovacs**[iD,*]

The Department of Chemistry, University of Washington, Box 351700, Seattle, Washington 98195-1700, United States

Abstract

Cysteinate oxygenation is intimately tied to the function of both cysteine dioxygenases (CDOs) and nitrile hydratases (NHases), and yet the mechanisms by which sulfurs are oxidized by these enzymes are unknown, in part because intermediates have yet to be observed. Herein, we report a five-coordinate bis-thiolate ligated Fe(III) complex, $[Fe^{III}(S_2{}^{Me2}N_3\text{-}(Pr,Pr))]^+$ (**2**), that reacts with oxo atom donors (PhIO, IBX-ester, and H_2O_2) to afford a rare example of a singly oxygenated sulfenate, $[Fe^{III}(\eta^2\text{-}S^{Me2}O)(S^{Me2})N_3(Pr,Pr)]^+$ (**5**), resembling both a proposed intermediate in the CDO catalytic cycle and the essential NHase Fe-$S(O)^{Cys114}$ proposed to be intimately involved in nitrile hydrolysis. Comparison of the reactivity of **2** with that of a more electron-rich, crystallographically characterized derivative, $[Fe^{III}S_2{}^{Me2}N^{Me}N_2{}^{amide}(Pr,Pr)]^-$ (**8**), shows that oxo atom donor reactivity correlates with the metal ion's ability to bind exogenous ligands. Density functional theory calculations suggest that the mechanism of S-oxygenation does not proceed via direct attack at the thiolate sulfurs; the average spin-density on the thiolate sulfurs is approximately the same for **2** and **8**, and Mulliken charges on the sulfurs of **8** are roughly twice those of **2**, implying that **8** should be more susceptible to sulfur oxidation. Carboxamide-ligated **8** is shown to be unreactive towards oxo atom donors, in contrast to imine-ligated **2**. Azide (N_3^-) is shown to inhibit sulfur oxidation with **2**, and a green intermediate is observed, which then slowly converts to sulfenate-ligated **5**. This suggests that the mechanism of sulfur oxidation involves initial coordination of the oxo atom donor to the metal ion. Whether the green intermediate is an oxo atom donor adduct, Fe-O═I-Ph, or an Fe(V)═O remains to be determined.

[*]**Corresponding Author** kovacs@chem.washington.edu.

[§]UW staff crystallographer.

ORCID[iD]

Julie A. Kovacs: 0000-0003-2358-1269

ASSOCIATED CONTENT

Supporting Information

The Supporting Information is available free of charge on the ACS Publications website at DOI: 10.1021/jacs.6b03512.

X-ray crystallographic data for **5** (CIF)

X-ray crystallographic data for **8** (CIF)

Experimental details regarding the synthesis and characterization of the $[(Pr,Pr)(N^{Me}HN^{amide}{}_2{}^{Me}SH)_2)]$. HCl ligand; ESI-MS, IR, and CV of **5**; ESI-MS, IR, CV, aqueous electronic absorption, and EPR spectra of **8**; electronic spectral evidence for the formation of **5** via a green metastable intermediate; crystallographic tables for **5** and **8**; and metrical parameters for DFT-optimized structures, including Scheme S-1, Figures S1-1–Figure S-14, and Tables S-1–S-11 (PDF)

The authors declare no competing financial interest.

Graphical abstract

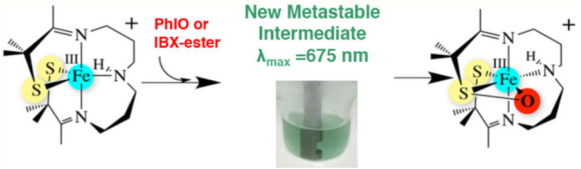

INTRODUCTION

Cysteine dioxygenases (CDOs) are non-heme Fe-enzymes that catalyze the O_2-promoted oxygenation of cysteinate ($^{cys}S^-$) to cysteine sulfinic acid ($^{cys}SO_2^-$).[1–8] A singly oxygenated cysteine sulfenate ($^{cys}SO^-$) is proposed to be involved as an intermediate. High levels of cysteine can cause rheumatoid arthritis, and neurological disorders such as Parkinson's disease and Alzheimer's disease.[5, 9] Thus, having a mechanism for its degradation is important to human health. The CDO enzyme has also been shown to suppress tumor growth by combatting the tumor's defense against reactive oxygen species.[10] An epigenetic event can turn off CDO tumor suppression,[11] however, via methylation of the gene responsible for the biosynthesis of CDO. Methylated CDO genes are found in ~60% of breast cancers and correlate with the progression of the disease and outcome.[12] The CDO mechanism (Figure 1) is proposed to involve cysteine binding to the metal ion, followed by O_2 binding, *cis* to the $^{cys}S^-$, to afford an Fe^{III}-$O_2^{\bullet-}$intermediate (**A**). The superoxo radical is then proposed to couple with the Fe^{II}-$^{cys}S^{\bullet}$↔ Fe^{III}-$^{cys}S^-$ sulfur to afford a fourmembered-ring structure, RS-Fe^{II}-O-O (**B**).[5] This step is unprecedented, in part because there are very few reported Fe^{III}-$O_2^{\bullet-}$,[8, 13, 14] but more importantly, because none have RS^-ligands in the coordination sphere. Upon heterolytic cleavage of the O-O bond, a high-valent iron−oxo intermediate with a singly oxygenated sulfenate, (RSO)Fe^{IV}═O (**C**), is proposed to form, which undergoes *cis*-migration to afford the final doubly oxygenated cysteine sulfinate.[1, 5] Although theoretical calculations have indicated that the direct involvement of the metal ion of CDO provides a lower energy pathway to sulfur oxygenation,[1, 5] this has not been experimentally proven. Intermediates **A–C** (Figure 1) have yet to be observed. The lack of spectroscopic data for any of the proposed CDO intermediates has made it impossible to calibrate theoretical calculations.[5]

Dioxygen has been shown to react with small-molecule iron thiolate (RS^-) complexes to afford doubly or triply oxygenated thiolates.[15–20] For example, cysteinate-ligated $TpFe^{II}S^{cys}$ reacts with O_2 to afford $^{cys}SO_2^-$ (the product of CDO[5]); however, no intermediates were observed.[21] Iron complexes containing a non-tethered, monodentate RS ligand *trans* to the O_2 binding site have been shown to react with O_2 to afford an Fe^{IV}═O + RSSR, [3, 22] in contrast to *cis*-thiolate-ligated complexes, which have been shown to react with O_2 to afford doubly (RSO_2-Fe) or triply (RSO_3-Fe) oxygenated derivatives.[1–4, 22, 23] Singly oxygenated RSO-Fe sulfenate intermediates are not observed in these cases. Whether these reactions are metal-mediated, or involve direct attack of O_2 at sulfur, has not been determined, although the orientation dependence would suggest the former. The mechanism of O_2-induced oxygenation of Ni-thiolate complexes, on the other hand, has been shown to involve direct attack by O_2 at the thiolate sulfurs.[24]

Oxygenated cysteinates have been shown to play a growing number of diverse roles in cellular processes, including T-cell activation, redox signaling in mammalian cells,[25] signal transduction, oxygen metabolism, oxidative stress response, and transcriptional regulation.[25, 26] They are also required for enzyme activity in some cases (e.g, nitrile hydratase (NHase),[27–31] NADH peroxidase,[32] and peroxiredoxins[33]). Nitrile hydratases are a class of thiolate-ligated non-heme iron enzymes for which cysteinate oxygenation is intimately tied to function. These enzymes, which catalyze the enantioselective hydrolysis of nitriles to amides,[34–38] contain an Fe(III) (or Co(III)) active site ligated by three cysteinates, two of which are post-translationally modified (Scheme 1), one to a sulfenic acid (^{114}Cys-S-OH) [31, 39, 40] and the other to a sulfinate (^{112}Cys-SO_2^-).[41] Sulfur K-edge X-ray absorption spectroscopic studies have shown that the NHase sulfenic acid residue is protonated,[39] whereas the sulfinate (RSO_2^-) remains unprotonated.[39] The enzyme becomes inactive when a second oxygen atom is added to the sulfenic acid,^{114}Cys-S-OH, implying that it plays a specific role in catalysis.[42] This is supported by time-resolved crystallography[43] and crystallographic characterization of ^{114}Cys-S-bound inhibitors.[31] Coupled with theoretical calculations,[27] these experimental data provide evidence that *the sulfenate oxygen is intimately involved in the NHase mechanism*. The mechanism by which post-translationally modified NHase sulfenate and sulfinate oxygens are inserted has been proposed to involve O_2-induced formation of a thiolate-ligated high-valent oxo intermediate.[22, 29] There are no experimental data available to verify this possibility, however.

Singly oxygenated sulfenates are difficult to trap,[26, 44–47] even when they are coordinated to a metal ion (i.e., M-S(R)-O^-). [24, 48, 49] There are significantly more examples of doubly oxygenated metal-sulfinate (RSO_2^-) complexes. [15–20] Examples of singly oxygenated RS═O or RS-OH compounds include $[Co^{III}(\eta^2\text{-}SO)(SO_2)N_3(Pr,Pr)]^+$ (Scheme 2),[49] $[Fe^{III}(ADIT)\text{-}(ADIT\text{-}O)]^+$ (**1**),[48] and $[Fe^{III}(ADIT)(ADIT\text{-}OH)]^{2+}$.[48]

In order to understand how thiolates promote O_2 activation[50–52] and tune the electronic, magnetic, and reactivity properties of peroxo, oxo, and hydroxo intermediates, we have been exploring the reactivity of coordinatively unsaturated thiolate-ligated Fe (and Mn) complexes with dioxygen and its reduced derivatives.[51, 53–59] Although an open coordination site is required for O_2 binding, thiolates are known to intercept open coordination sites by forming intermolecular M-SR-M bridges, resulting in oligomerization. Despite this, we,[17, 51, 54, 59–67] and others,[2, 3, 16, 18, 68–70] have synthesized a variety of coordinatively unsaturated mononuclear thiolate-ligated iron complexes that are capable of binding small molecules. For example, thiolate-ligated $[Fe^{II}(N_4S^{Me2}\text{-}(tren))]^+$,[54, 71] and bis-thiolate-ligated $[Fe^{III}(S_2{}^{Me2}N_3(Pr,Pr))]$ (**2**,[63] Scheme 3), are five-coordinate, and contain flexible ligands capable of accommodating a sixth ligand,[62, 63, 72] as well as a variety of metal ions, in multiple oxidation states.[59, 60, 62, 63, 72–74] Both ligands constrain the geometry so that added “substrates” are forced to bind cis to a thiolate (e.g., structures **3** and **4**, Scheme 4).[64, 65, 75, 76] For example, superoxide (O_2^-) reacts with reduced $[Fe^{II}(N_4S^{Me2}(tren))]^+$ at low temperatures in the presence of a proton donor[59, 75, 77] to afford a metastable, low-spin ($S = 1/2$; $g_\perp = 2.14$; $g_\parallel = 1.97$) hydroperoxo intermediate, $[Fe^{III}(N_4S^{Me2}(tren))(OOH)]^+$ (**3**, Scheme 4; $\upsilon_{O\text{-}O} = 784\ cm^{-1}$).[54] Bis-thiolate ligated **2** (Scheme 3) was shown to bind L = N_3^- (**4**) and NO *cis* to one of the thiolates and *trans* to

the other (Scheme 4).[63, 78] Despite the π-donor properties of RS^- ligands, the highly covalent Fe−S bonds of oxidized $[Fe^{III}(N_4S^{Me2}(tren))L]^+$ (L = MeCN, HOO^-(**3**)),[54, 64, 65] $[Fe^{III}(S_2{}^{Me2}N_3(Pr,Pr))]^+$ (**2**), and $[Fe^{III}(S_2{}^{Me2}N_3$-(Pr,Pr))$(N_3)]$ (**4**)[63] were all shown to favor a low-spin state (S = 1/2), due to the nephalauxetic effect.[79] The *trans*-thiolate of **4** was shown to labilize the azide[63], thereby promoting reversible L-binding.[80] Herein we examine the reactivity of bis-thiolate-ligated $[Fe^{III}(S_2{}^{Me2}N_3(Pr,Pr))]^+$ (**2**, Scheme 3) with oxo atom donors in order to determine how the presence of both a *cis*-and *trans*-thiolate influences electronic structure and reactivity.

EXPERIMENTAL SECTION

General Methods

All reactions were performed under an atmosphere of dinitrogen in a glovebox, using standard Schlenk techniques, or using a custom-made solution cell equipped with a threaded glass connector sized to fit a dip probe. Reagents purchased from commercial vendors were of the highest purity available and used without further purification. Toluene, tetrahydrofuran (THF), diethyl ether (Et_2O), and acetonitrile (MeCN) were rigorously degassed and purified using solvent purification columns housed in a custom stainless steel cabinet, dispensed via a stainless steel Schlenk-line (GlassContour). Methanol (MeOH) and ethanol (EtOH) were distilled from magnesium methoxide or ethoxide and degassed prior to use. Methylene chloride (DCM) was distilled from CaH_2 and degassed prior to use. ^{1}H NMR spectra were recorded on Bruker AV 300 or Bruker AV 301 FT-NMR spectrometers and are referenced to an external standard of tetramethylsilane (paramagnetic compounds) or to residual protio-solvent (diamagnetic compounds). Chemical shifts are reported in ppm, and coupling constants (J) are in Hz. EPR spectra were recorded on a Bruker EMX CW-EPR spectrometer operating at X-band frequency at 7 K. IR spectra were recorded on a PerkinElmer 1700 FT-IR spectrometer as KBr pellets. Cyclic voltammograms were recorded in MeCN (100 mM $Bu^n{}_4N(PF_6)$ solutions) on a PAR 273 potentiostat utilizing a glassy carbon working electrode, platinum auxiliary electrode, and a saturated calomel electrode (SCE) reference electrode. Magnetic moments (solution state) were obtained using Evans's method as modified for super-conducting solenoids.[81, 82] Temperatures were obtained using Van Geet's method.[83] Solid-state magnetic measurements were obtained with polycrystalline samples in gel-caps using a Quantum Design MPMS S5 SQUID magnetometer. Ambient-temperature electronic absorption spectra were recorded on a Hewlett-Packard model 8450 spectrometer, interfaced to an IBM personal computer. Low-temperature electronic absorption spectra were recorded using a Varian Cary 50 spectrophotometer equipped with a fiber optic cable connected to a "dip" attenuated total reflection probe (C-technologies), with a custom-built two-neck solution sample holder equipped with a threaded glass connector (sized to fit the dip probe). Elemental analyses were performed by Galbraith Labs, Knoxville, TN, and Atlantic Microlabs, Norcross, GA. Thiolate-ligated $[Fe^{III}(S_2{}^{Me2}N_3$-(Pr,Pr))$](PF_6)$ (**2**) was synthesized as previously described.[63]

Synthesis of [$Fe^{III}(\eta^2$-$S^{Me2}O)(S^{Me2}N_3$(Pr,Pr)](PF$_6$) (5) via the Addition of PhIO to 2

To a stirred solution of [$Fe^{III}(S_2{}^{Me2}N_3$-(Pr,Pr))](PF$_6$) (**2**) (275 mg, 0.52 mmol) in MeOH (20 mL) at −35 °C was added dropwise a 2 mL MeOH solution containing 1.2 equiv of iodosobenzene (PhIO) (137 mg, 0.62 mmol). The solution was allowed to stir for 1 h at −35 °C, and then stored in the freezer overnight. After filtration, the volume was reduced to 3 mL, layered with 25 mL of Et_2O, and cooled to −35 °C overnight to afford **5** (153 mg, 0.28 mmol, 54%) as a pink crystalline solid. Electronic absorption (CH_3CN): λ_{max} (ε, M^{-1} cm^{-1}) = 333 (4410), 510 (1540) nm; (MeOH): λ_{max} (ε, M^{-1} cm^{-1}) = 325 (4870), 510 (1700), 760 (248) nm (Figure S-1). IR (KBr pellet) ν (cm^{-1}): 1625 (C═N); 1024 (S-O). Reduction potential (MeCN): $E_{p,c}$ = −0.960 V (irrev.) vs SCE. Solution magnetic moment (310.2 K; MeOH): μ_{eff} = 1.99 μ_B. EPR (DCM/toluene glass (1:1), 7 K): g_1 = 2.17, g_2 = 2.11, g_3 = 1.98. ESI-MS calcd for $[FeC_{16}N_3S_2H_{31}O]^+$: 401.3; found: 401.2. Anal. Calcd for $FeC_{16}H_{31}N_3OS_2PF_6$: C, 35.2; H, 5.7; N, 7.7. Found: C, 35.39; H, 5.57; N, 7.77.

Formation of [$Fe^{III}(\eta^2$-$S^{Me2}O)(S^{Me2}N_3$(Pr,Pr)](PF$_6$) (5) via the Addition of Hydrogen Peroxide to 2

Oxidized **2** (5 mg, 0.01 mmol) was dissolved in 20 mL of MeOH and placed in a sealed UV–vis dip-probe cell under a N_2 atmosphere. To this was added 1.0 equiv of H_2O_2 (1 μL of a 30% aqueous solution, 0.01 mmol) at room temperature via syringe to afford a pink air-stable compound (λ_{max}= 510 nm (1540 M^{-1} cm^{-1}); ESI-MS (M+1): 401). Complex **5** is stable both at room temperature and in air.

Synthesis of (Et_4N)[$Fe^{III}S_2{}^{Me2}N^{Me}N_2{}^{amide}$(Pr,Pr)] (8)

To a stirred solution of $(HS^{Me})_2(N^{Me})(HN^{amide})_2$(Pr,Pr)·HCl (C, see Supporting Information for synthesis) (100 mg, 0.26 mmol) in MeOH (5 mL) at −35 °C was added dropwise a pre-cooled (−35 °C) solution of (Et_4N)[$FeCl_4$] (85 mg, 0.26 mmol) in MeOH (3 mL). A pre-cooled (−35 °C) solution of NaOMe (70 mg, 1.3 mmol) in MeOH (5 mL) was then added, and the resulting reaction mixture was allowed to stir overnight at ambient temperature. The intense olive green solution was filtered and concentrated to dryness. The solid was re-dissolved in MeCN and filtered. The filtrate was concentrated to a minimum amount of MeCN (~2 mL), layered with 10 mL of Et_2O, and cooled to −35 °C overnight to afford 8 (110 mg, 0.21 mmol, 80%) as a dark green crystalline solid. Electronic absorption (CH_3CN): λ_{max} (ε, M^{-1} cm^{-1}) = 352 (8210), 428 (3590), 581 (1280) nm; (MeOH): λ_{max} (ε, M^{-1} cm^{-1}) = 348 (8150), 588 (1210) nm; (H_2O): λ_{max} (ε, M^{-1} cm^{-1}) = 352 (8060), 584 (1530) nm. IR (KBr pellet) ν (cm^{-1}): 1564 (C═O). $E_{1/2}$ (MeCN) = −1.51 V vs SCE. Solution magnetic moment (298 K; MeOH): μ_{eff} = 3.75 μ_B. EPR (MeOH/EtOH glass (9:1), 9 K): g_1 = 4.72, g_2 = 2.82, g_3 = 1.92. ESI-MS calcd for $[FeC_{13}H_{21}N_2O_2S_3]^-$: 389.4, found: 389.3. Anal. Calcd for $FeC_{23}H_{47}N_4O_2S_2$: C, 52.0; H, 8.9; N, 10.5. Found: C, 52.3; H, 8.87; N, 10.49.

Formation of a Green Intermediate via the Addition of IBX-Ester to 2

A 0.238 mM solution of **2** was prepared in 5 mL of MeOH under an inert atmosphere in a drybox. The resulting solution was transferred via gastight syringe to a custom-made two-neck vial equipped with a septum cap and threaded dip-probe feed-through adaptor that had

previously been purged with argon and contained a stir bar. This solution was cooled in an acetone/dry ice bath to −73 °C. To this was added 10 equiv of IBX-ester (isopropyl 2-iodoxybenzoate) (50 μL of 238 mM solution of IBX-ester in MeOH), resulting in the formation of a metastable green intermediate (λ_{max} = 675 nm).

Formation of a Green Intermediate via the Addition of PhIO to 2

A 0.238 mM solution of **2** was prepared in 5 mL of MeOH or THF under an inert atmosphere in a drybox. The resulting solution was transferred via gastight syringe to a custom-made two-neck vial equipped with a septum cap and threaded dip-probe feed-through adaptor that had previously been purged with argon and contained a stir bar. This solution was cooled in an acetone/dry ice bath to −73 °C. To this was added 1–4 equiv of PhIO (50–200 μL of 23.8 mM solution in MeOH), resulting in the formation of a metastable intermediate (λ_{max} = 675 nm).

DFT Calculations

All geometry optimizations were performed utilizing the ORCA v.3.0 quantum chemistry package[84] and originated from X-ray crystallographic coordinates. The BP86 functional,[85, 86] with the resolution of identity approximation (RI),[87] dispersion correction (D3BJ),[88] and zeroth-order regular approximation for relativistic effects (ZORA),[89] was employed, using a dense integration grid (Grid4), def2-TZVP basis set,[90] and def2-TZVP/J auxiliary basis set.[87] In addition, the conductor-like screening model (COSMO), using acetonitrile (ε = 37.5) as the solvent,[91] was employed. All optimized geometries were visualized using Avogadro.

X-ray Crystallographic Structure Determination

A red crystal plate, 0.24 × 0.24 × 0.05 mm, of **5** was mounted on a glass capillary with oil. Data were collected at −143 °C. The crystal-to-detector distance was set to 30 mm, and exposure time was 30 s per degree for all data sets, with a scan width of 1.4°. The data collection was 89.1% complete to 28.34° and 96.1% complete to 25° in θ. A total of 63 733 partial and complete reflections were collected, covering the indices h = −16 to 16, k = −18 to 20, l = −19 to 19. A total of 5215 reflections were symmetry independent, and the R_{int} = 0.0698 indicated that the data were of average quality (0.07). Indexing and unit cell refinements indicated a monoclinic P lattice in the space group $P2_1/c$ (No. 14).

A black crystal prism, 0.48 × 0.44 × 0.36 mm, of 8 was mounted on a glass capillary with oil. Data were collected at −143 °C. The crystal-to-detector distance was set to 40 mm, and exposure time was 20 s per degree for all sets, with a scan width of 1.5°. The data collection was 94.5% complete to 28.63° and 99.8% complete to 25° in θ. A total of 41 494 partial and complete reflections were collected, covering the indices h = −23 to 23, k = −11 to 11, l = −23 to 23. A total of 6353 reflections were symmetry independent, and the R_{int} = 0.063 indicated that the data were of average quality (0.07). Indexing and unit cell refinement indicated an orthorhombic P lattice in the space group $Pna2_1$ (No. 33).

The data for both **5** and **8** were integrated and scaled using Denzohkl-SCALEPACK, and an absorption correction was performed using SORTAV. Scattering factors were obtained from

Waasmair and Kirfel.[92] Solution by direct methods (SIR97) produced a complete heavy-atom phasing model consistent with the proposed structures. All non-hydrogen atoms were refined anisotropically by full-matrix least-squares methods, and all hydrogen atoms were then located using a riding model. Crystal data for **5** and **8** are presented in Table 1; CIF files for **5** and **8** are available as Supporting Information. Selected bond distances and angles are assembled in Table 2 in the following section.

RESULTS AND DISCUSSION

Addition of 1.2 equiv of PhIO to five-coordinate $[Fe^{III}(S_2{}^{Me2}N_3(Pr,Pr))]^+$ (**2**)[63] at ambient temperatures induces a color change from orange to magenta, and causes the S→Fe charge-transfer (CT) band in the electronic absorption spectrum, at 415 nm (4200 M^{-1} cm^{-1}) , to disappear, and a new band to grow in at 510 (1540) nm (Figure 2). A red-shifted absorption band would be consistent with an increase in metal ion Lewis acidity, as a consequence of oxo atom addition. Electrospray ionization mass spectrometry (ESI-MS) of this magenta species, **5**, shows a peak at *m/z* = 401, corresponding to the parent ion M + 16 (Figure S-2), consistent with the addition of a single oxygen atom. Addition of 1 equiv of H_2O_2(aq) to **2** in MeOH (Figure S-3) affords an identical magenta-colored species (**5**, λ_{max} = 510 nm (1540 M^{-1} cm^{-1})), with an identical ESI mass spectrum, indicative of the addition of a single oxygen atom. Single oxo atom addition to **2** would be consistent with the formation of either a high-valent iron oxo or an iron-sulfenate (FeS(R)-O^-) species. The low-temperature (7 K), perpendicular-mode EPR spectrum of **5** (Figure 3) reproducibly displays an intense rhombic signal with *g*-values of 2.16, 2.10, and 1.97, indicative of an $S = 1/2$ ground state. The precursor to **5**, $[Fe^{III}(S_2{}^{Me2}N_3(Pr,Pr))]^+$ (**2**), is also low-spin $S = 1/2$, but has distinctly different *g*-values (g = 2.20, 2.15, and 2.00).[63] The ambient-temperature MeOH solution magnetic moment of **5** (μ_{eff} = 1.99 μ_B) is also consistent with an $S = 1/2$ spin state and indicates that there are no thermally accessible higher spin states in the range 7–300 K. In contrast, **2** has an ambient-temperature magnetic moment of μ_{eff} = 3.5 μ_B, reflecting the thermal accessibility of an $S = 3/2$ excited state.[63] The $S = 1/2$ ground state of **5** would be consistent with either an Fe(V)[93–96] or an Fe(III) oxidation state,[48, 54, 59–61, 63, 66, 79, 99] but inconsistent with an even-spin, $S = 1$ or $S = 2$ system, thereby ruling out an Fe(IV)═O.

The redox properties of **5** also differ from those of **2**. Whereas five-coordinate **2** is reversibly reduced at a potential of $E_{1/2}$ = −425 mV vs SCE (Figure 4), **5** is irreversibly reduced at a significantly more negative potential (E_{pc} = −958 mV, E_{pa}= −690 mV vs SCE; Figure S-4). Oxygen atom addition therefore increases the stability of the Fe^{3+} oxidation state. Oxygenation at sulfur would be expected to shift the potential in the opposite direction, given that it would decrease the electron-donating properties of the sulfur, unless, of course, the unmodified thiolate overcompensates for the increase in Lewis acidity by forming a more covalent unmodified Fe–SR bond.[48] If the latter were the case, then the S→Fe CT band would blue-shift,[48] as opposed to the red-shift shown in Figure 2. On the other hand, ferric ions are more stable in a six-coordinate environment, relative to a five-coordinate environment, perhaps suggesting that oxo atom addition involves the metal ion.

Iodosyl benzene (PhIO) typically promotes two-electron chemistry, and has been shown to convert Fe(II) compounds to Fe(IV)═O compounds.[98–101] There are fewer examples of

Fe(III) compounds that are reactive toward oxo atom donors, such as PhIO (Figure 2). [102–104] One example of the latter involves the addition of PhIO to cytochrome P450 in its Fe(III) resting state, to afford (por/^{cys}S)Fe(V)═O (compound I).[105] The oxidizing equivalents of P450 compound I have been shown to be delocalized over both the redox-active porphyrin (por) and the redox-active thiolate ligands. [106–111] Hydrogen peroxide (H_2O_2) has also been shown to convert Fe(III) compounds to Fe(V)═O species,[112, 113] or its redox equivalent.[107, 109, 111] In contrast to Fe(IV)═O compounds, [52, 98, 114–123] however, very few synthetic non-heme Fe(V)═O species have been observed. [93, 95, 96, 104, 113, 124] The most thoroughly characterized example, [Fe(V)(TAML)(O)]$^{-}$, incorporates an electron-donating tetra-anionic carboxamide ligand (*vide inf ra*), TAML[4–93, 95, 104, 125, 126].

The IR spectrum of **5** contains a stretch at ν = 1024 cm^{-1} (Figure S-5) that is absent in the IR spectrum of **2**. This stretching frequency would be extremely high for an Fe(V)═O ($\nu_{Fe═O}$ = 798–828 cm^{-1})[96, 127] and is somewhat above the usual range ($\nu_{S═O}$ = 970–900 cm^{-1})[24, 35, 46, 128–130] for a metal-sulfenate complex Sulfenate $\nu_{S═O}$ stretches have, however, previously been shown to shift out of the usual range if the RS═O is η^2 -coordinated to a metal ion.[49, 131] For example, sulfenate/sufinate-ligated [Co^{III}(η^2-SO)(SO_2)N_3(Pr,Pr)]$^{+}$ (Scheme 2) has a sulfenate $\nu_{S═O}$ stretch at 1066 cm^{-1}.[49]

X-ray Structure of [Fe^{III}(η^2-S^{Me2}O)(S^{Me2})N_3(Pr,Pr)](PF_6) (5)

The identity of the product, **5**, formed in the reaction between **2** and PhIO (or H_2O_2) was ultimately determined by X-ray crystallography. Single crystals of **5** were grown at −30 °C by layering Et_2O onto an MeCN solution. As shown in the ORTEP diagram of Figure 5, the single oxygen atom O(1) adds ~*trans* (O(1)–Fe–S(2) = 152.3(2)°) to one of the thiolate sulfurs, S(2), and forms a bond to the cis-thiolate S(1), affording an **η^2**-coordinated sulfenate, [Fe^{III}(**η^2**-S^{Me2}O)(S^{Me2})-N_3(Pr,Pr)]$^{+}$ (**5**). A similar side-on sulfenate (**η^2**-RSO^{-}) binding mode was observed previously in [Co^{III}(η^2-SO)(SO_2)N_3-(Pr,Pr)]$^{+}$ (Scheme 2).[49] As mentioned earlier, singly oxygenated metal sulfenates (RSO^{-}) are rare, [24, 48, 49] since they tend to be more reactive than their thiolate precursor. [26, 46, 47, 49] There are significantly more examples of doubly oxygenated, structurally rearranged, oxygen-bound metal-sulfinate (RSO_2^{-}) complexes.[16–20]

Comparison of structure **5** (Figure 5) with that of its [Fe^{III}($S_2^{Me2}N_3$(Pr,Pr))]$^{+}$ (**2**) precursor (Table 2) shows that the singly oxygenated Fe–S(1) bond of **5** elongates only slightly as a result of oxygen atom addition (from 2.133(2) Å in **2** to 2.142(2) Å in **5**). One would have expected a more dramatic change in bond length. The Fe–S(2) bond, on the other hand, decreases in length from 2.161(2) Å in **2** to 2.148(2) Å in **5**, indicating that the unmodified thiolate compensates for the shifting of electron density away from the metal ion toward the oxygen atom. This compensatory effect was observed previously with [Fe^{III}(ADIT)(ADIT-O)]$^{+}$ (**1**; Scheme 2).[48] The sulfenate S(1)–O(1) bond in **5** (1.447 Å; Table 2) is slightly shorter than in the few known sulfenate complexes (range: 1.50–1.60 Å),[24, 46, 131] including that of [Co^{III}((η^2-SO)(SO_2)N_3(Pr,Pr))]$^{+}$ (Scheme 2) (S(1)-O(1), 1.548(3) Å).[49]

Synthesis of a More Electron-Rich Derivative of 2

In order to provide an even more electron-rich environment, analogous to that of the $TAML^{4-}$ ligand shown previously to stabilize an Fe(V)═O,[93] we synthesized (Scheme S-1) the tetra-anionic carboxamide ligand $[(Pr,Pr)(N^{Me}N^{amide}{}_2S^{Me}{}_2)]^{4-}$ (Figures S-6–S-9) and its corresponding Fe-complex (Scheme 5). As mentioned earlier, the preferred $2e^-$ chemistry of PhIO makes it conceivable that oxo atom addition to Fe(III)-**2** results in the formation of an unobserved metastable Fe(V)═O intermediate along the reaction pathway to **5**. The highly covalent Fe–S bonds would help to delocalize the oxidizing equivalents, thereby making the higher-valent state accessible. The placement of a nucleophilic thiolate *cis* to an electrophilic oxo would facilitate rapid intramolecular trapping of the oxo via the formation of a S–O bond. A similar reaction sequence was recently observed to convert a sulfur-bound substrate analogue of isopenicillin-N-synthase to an $Fe^{II}((\eta^2\text{-SO})$,[132] and may be the mechanism by which the catalytically important sulfenate is inserted into the Fe-NHase active site.[27]

Bis-thiolate/carboxamide-ligated $[Fe^{III}S_2{}^{Me2}N^{Me}N_2{}^{amide}\text{-}(Pr,Pr)]^-$ (**8**) displays a $\nu_{C=O}$ stretch at 1564 cm^{-1} (Figure S-11) and a parent ion peak in the negative-mode ESI-MS (Figure S-10). This would be consistent with the structure shown in Scheme 5, which incorporates anionic carboxamides in place of the neutral imines of **2**. X-ray-quality crystals of $(Et_4N)[Fe^{III}S_2{}^{Me2}N^{Me}\ N_2{}^{amide}(Pr,Pr)]$ (**8**) were obtained via slow vapor diffusion of Et_2O into an MeCN solution at −35 °C. As shown in the ORTEP diagram in Figure 6, the Fe^{3+} ion of **8** maintains a five-coordinate structure, despite being crystallized from a coordinating solvent (MeCN), and resides in a highly distorted N_3S_2 environment ($\tau = 0.56$) halfway between trigonal bipyramidal and square pyramidal. The Fe^{3+} ion is ligated by two *cis*-thiolate sulfurs and a tertiary amine (N(2)) in the equatorial plane, and two *trans*-carboxamide nitrogens (N(1), N(3)) in apical positions. Key bond distances and angles are compared with those of its cationic imine analogue **2** in Table 2. The incorporation of anionic carboxamides in **8**, in place of the neutral imines of **2**, causes the mean Fe–S bond distance to significantly elongate (from 2.147 Å in 2 to 2.22 Å in **8**). A similar increase in Fe–S bond lengths (from 2.189 to 2.219 Å) is seen upon replacement of the neutral imines in $[Fe^{III}(tame\text{-}N_3)S_2{}^{Me2})]^+$ with anionic carboxamides in $[Fe^{III}\text{-}((tame\text{-}N_2S)S_2{}^{Me2})]^{2-}$.[17] The S–Fe–S angle (144°) in **8** is significantly wider than that of **2** (121°), as well as imine-ligated $[Fe^{III}(S_2{}^{Me2}N_3(Et,Pr))]^+$ (105°).[61]

Carboxamide-ligated **8** is soluble in a variety solvents, including H_2O, forms intense olive green-colored solutions, and displays a solvent-independent electronic absorption spectrum with bands at λ_{max} = 352 (8060), 450 (sh), and 584 (1530) nm, indicating that solvents (MeCN, MeOH, H_2O (Figure 7)) do not coordinate to the metal ion. The redox potential of anionic **8** (−1.51 V vs SCE; Figure 8) is shifted by over 1 V, relative to that of cationic imine-ligated **2** ($E_{1/2}$ = −425 mV vs SCE, Figure 4), demonstrating that carboxamide ligands provide significant stability to the Fe^{3+} oxidation state.[133]

As shown by fits to the inverse magnetic susceptibility ($1/\chi_m$) versus temperature plot of Figure 9, and low-temperature (7 K) perpendicular-mode EPR (g = 4.72, 2.82, 1.92; (Figure S-12), bis-thiolate-ligated **8** has an S = 3/2 ground state, and maintains this spin state over a wide temperature range in the solid state and in frozen solution. The ambient-temperature

MeCN solution magnetic moment of μ_{eff} = 3.75 μ_B indicates that **8** maintains this spin state in solution. In contrast, imine-ligated **2** has an S = 1/2 ground state, with a thermally accessible S = 3/2 state that is ~23% populated at ambient temperature and 11% populated at T = −80 °C. Spin states have been shown to influence reactivity in profound ways.[134, 135]

Comparison of the Reactivity Properties of Carbox-amide-Ligated 8 versus Imine-Ligated 2

In contrast to **2**, carboxamide-ligated **8** does *not* react with oxo atom donors PhIO or H_2O_2, under any conditions, even with a ~ 1000-fold excess of oxidant, and over a wide temperature range (−78 to +25 °C). One would have anticipated that the thiolates of **8** would be more readily oxygenated, given the anionic molecular charge, and expected increase in electron density on the thiolate sulfurs. Given the similarity of its ligand environment to that of [Fe(V)(TAML)(O)]$^-$, one would have also anticipated that an Fe(V)═O might be stabilized, possibly to the point where it might be observable, prior to intramolecular trapping and S−O bond formation. If, on the other hand, sulfur oxidation involves direct attack at the thiolate sulfurs, then one would also expect carboxamide-ligated **8** to be more reactive toward oxo atom donors than **2**, because the thiolate sulfurs should carry more negative charge. In order to determine whether the latter is indeed the case, and quantify this difference if it exists, we turned to theoretical calculations. Density functional theory (DFT) calculations were performed on both **2** and **8**, and metrical parameters of the DFT-optimized geometry are reproduced to 0.04 Å of the crystallographically-determined bond lengths (Table S-1). Based on these calculations, the Mulliken charges on the sulfurs of anionic **8** (−0.484 for S(1), −0.488 for S(2)) were found to be roughly twice those of cationic **2** (−0.288 for S(1), −0.245 for S(2)). The longer Fe-S bond distances in **8**, relative to **2**, would be consistent with this. The calculated average spin-density on the thiolate sulfurs is approximately the same for **2** (0.12) and **8** (0.15). Theoretical calculations therefore suggest that, if oxo atom donors were to directly attack the thiolate sulfur in a 2e–process, then carboxamide-ligated **8** would be more reactive than imine-ligated **2**, when in fact the opposite is observed. If a 1e$^-$ radical process, involving direct attack at the sulfurs, were involved, then the two complexes **2** and **8** should be equally reactive. Oxo atom donor reactivity does, on the other hand, correlate with ligand binding properties. Despite its open coordination site, anionic **8** does *not* bind neutral (pyridine, MeCN) or anionic (N_3^-, CN^-) ligands, even when added in excess (>100 equiv) at low temperatures (−40 to −78 °C), as determined using electronic absorption spectroscopy. This is likely due to the fact that a spin-state change would be required in order for five-coordinate **8** to convert to a six-coordinate structure. Whereas **8** is S = 3/2, six-coordinate, thiolate-ligated ferric complexes are predominantly low-spin S = 1/2.[39, 59, 79, 97, 136] As one would expect, calculated unpaired spindensity on the iron of **8** (2.59) is significantly larger than that of **2** (0.83), reflecting the S = 1/2 ground state of **2**. A Me group on N(2) of **8**, in place of the N(2)-H proton of **2**, also likely inhibits ligands from binding to **8**, since it would sterically clash with S(1) when the S(1)−Fe−N(2) bond angle decreased as a consequence of a the concomitant geometry change (~trigonal bipyriamidal → ~octahedral). Imine-ligated **2**, on the other hand, readily binds both N_3^- and NO to its open coordination site,[63, 78] in addition to reacting with oxo atom donors.

Thus, both correlations between sulfur oxidation and the molecule's affinity for a sixth ligand and ability to undergo a geometry change, and theoretical calculations, suggest that the mechanism of sulfur oxidation with **2** involves initial coordination of the oxo atom donor to the metal ion. Consistent with this, azide (N_3^-) is found to inhibit sulfur oxidation with **2**. If 1.2 equiv of N_3^- is added to **2** in THF at −73 °C, then the intense band at 415 (4200) nm, characteristic of **2**, is replaced by a band at 708 (1600) nm (Figure 10), characteristic of coordinatively saturated, azide-bound [Fe^{III}-($S_2^{Me2}N_3$(Pr,Pr))(N_3)] (**4**).[63] If, following the formation of azide-bound **4** in THF, 1.2 equiv of PhIO is added, no reaction is observed, even after prolonged reaction times (2 h). If, under the same conditions (−73 °C in THF), 1.2 equiv of PhIO is added to **2**, in the absence of N_3^-, then a metastable intermediate that converts to singly oxygenated [Fe^{III}(η^2-$S^{Me2}O$)($S^{Me2}N_3$(Pr,Pr)]$^+$ (**5**) (λ_{max} = 510 nm (1540 M^{-1} cm^{-1})) forms within minutes (*vide inf ra*). Thus, azide inhibits sulfur oxidation with **2**, presumably by preventing the oxo atom donor from binding to the metal ion. Consistent with this, we observe an intermediate in the oxo atom donor reaction in the absence of azide.

Observation of an Intermediate in the Reaction between Imine-Ligated 2 and Oxo Atom Donors PhIO and IBX-Ester

If the reaction between 10 equiv of PhIO and five-coordinate **2** is monitored by electronic absorption spectroscopy at low temperatures (−73 °C) in MeOH, a green intermediate with λ_{max} = 675 nm is observed (Figure S-13), which then slowly (*t* = 360 min, [**2**] = 0.238 mM) converts to sulfenate-ligated **5** (Figure S-14). As shown in Figure 11, an approximately identical intermediate (λ_{max} = 677 nm) is formed when IBX-ester is used in place of PhIO; however, its rate of conversion to sulfenate-ligated **5** (36 min, [**2**] = 0.238 mM) is significantly faster. IBX-ester contains an $I^V(=O)_2$ moiety[137], whereas PhIO contains an I^{III}=O moiety, providing a possible explanation for the differences in rates. The observation of intermediates in these reactions provides evidence that sulfur oxidation is assisted by the metal ion, and involves the initial binding of oxo-atom donors to Fe. Clear isosbestic points visible during the IBX reactions show that the new intermediate is stoichiometrically related to complex **2** and converts directly to the sulfenate complex **5**, thus eliminating the possibility of direct attack at sulfur. Whether the green intermediate is an oxo atom donor adduct, Fe-O=I-Ph, or an Fe(V)=O remains to be determined. Given how rare Fe-O=I-Ph[138, 139] and Fe(V)= O[93, 113, 124] species are, both possibilities are intriguing. The λ_{max} of our green intermediate (677 nm) is in the reported range for both an Fe(III)-O=I-Ph (λ_{max} = 660 nm)[139] and Fe(V)=O (λ_{max} = 630 nm (5400 M^{-1} cm^{-1})),[93, 104] consistent with either possibility. Iodosylarene adducts have been shown to be competent oxidants in oxygen-atom-transfer reactions.[138–142] Spectroscopic characterization of the green intermediate, along with the kinetics of both its formation and conversion to sulfenate-ligated **5**, will be the topic of a separate manuscript. Possible mechanisms for sulfur oxygenation would involve initial formation of an oxo atom donor adduct Fe-O=I-Ph that is either directly attacked by the adjacent nucleophilic sulfur, or that converts first to an Fe(V)=O, which is then rapidly and irreversibly trapped by the adjacent sulfur. The observation of one intermediate, as opposed to two, is consistent with either (a) rate-determining *cis*-migration of a thiolate sulfur to the oxo of a coordinated Fe-O=I-Ph, or (b) rate-determining cleavage of the I-O to afford an unobserved Fe(V)=O suggesting that the intermediate is likely an oxo atom donor adduct. The virtually identical electronic spectra associated with

the green intermediate, regardless of the nature of the oxo atom donor, is a bit puzzling, given that one would expect an Fe-O═I^{V}-Ph species to have electronic properties that differ from those of an Fe-O═I^{III}-Ph species. Inhibition studies, involving PhI, should help to distinguish mechanisms (a) and (b). The anticipated rapid rate of intramolecular trapping of an Fe(V)═O, relative to the likely rate of its formation, would suggest that it would be unobservable. This remains to be determined, however.

SUMMARY AND CONCLUSIONS

Cysteinate oxygenation is intimately tied to the function of both cysteinate dioxygenases (CDOs)[1–8] and nitrile hydratases (NHases).[31, 39–41] However, the mechanism by which sulfurs are oxidized by these enzymes is unknown, in part because intermediates have yet to be observed. Herein we show that oxo atom donors, PhIO and H_2O_2, react with coordinatively unsaturated $[Fe^{III}(S_2{}^{Me2}N_3(Pr,Pr))]^+$ (**2**) to afford a rare example of a singly oxygenated sulfenate, $[Fe^{III}(\eta^2\text{-}S^{Me2}O)\text{-}(S^{Me2})N_3(Pr,Pr)]^+$ (**5**). Sulfenate-ligated **5** is low-spin (S = 1/2; g = 2.17, 2.11, 1.98) and resembles both an intermediate proposed to form during CDO-catalyzed cysteine oxidation and the catalytically essential NHase Fe-S^{Cys114}-O, proposed to be intimately involved in its mechanism.[27, 31, 42, 43] In contrast to imine-ligated **2**, carboxamide-ligated $[Fe^{III}S_2{}^{Me2}N^{Me}N_2{}^{amide}\text{-}(Pr,Pr)]^-$ (**8**) was shown to be unreactive toward oxo atom donors PhIO or H_2O_2, under any conditions. DFT-calculated Mulliken charges on the sulfurs of anionic **8** were found to be roughly twice as negative as those of cationic **2**, indicating that if oxo atom donors were to directly attack the thiolate sulfur, then carboxamide-ligated **8** would be more reactive than imine-ligated **2**. Reactivity was shown to correlate with the metal ion's ability to bind exogenous ligands, and azide (N_3^-) was found to inhibit sulfur oxidation with **2**, suggesting that the mechanism of sulfur oxidation involves initial coordination of the oxo atom donor to the metal ion. Consistent with this, a green intermediate is observed to form, which then slowly converts to sulfenate-ligated **5**. Whether the green intermediate is an oxo atom donor adduct, Fe-O═I-Ph, or an Fe(V)═O remains to be determined. The placement of a nucleophilic thiolate *cis* to an electrophilic oxo would facilitate rapid intramolecular trapping of a high-valent oxo via the formation of an S–O bond. Although the direct involvement of the metal ion has been theoretically calculated to provide a lower energy pathway to sulfur oxygenation by CDO,[5] this has not been experimentally proven.[7]

Supplementary Material

Refer to Web version on PubMed Central for supplementary material.

Acknowledgments

This work was supported by the NIH (GM45881). P.L.-M. gratefully acknowledges support by an NIH pre-doctoral minority fellowship (F31 GM73583-01). We also gratefully acknowledge Stephen J. Lippard, and an anonymous donor for financial support, and Xiaosong Li and Joe Kasper for help with the DFT calculations.

REFERENCES

1. Kumar D, Sastry GN, Goldberg DP, de Visser SP. J. Phys. Chem. A. 2012; 116:582–591. [PubMed: 22091701]

2. McQuilken AC, Jiang Y, Siegler MA, Goldberg DP. J. Am. Chem. Soc. 2012; 134:8758–8761. [PubMed: 22578255]
3. Badiei YM, Siegler MA, Goldberg DP. J. Am. Chem. Soc. 2011; 133:1274–1277. [PubMed: 21207980]
4. Jiang Y, Widger LR, Kasper GD, Siegler MA, Goldberg DP. J. Am. Chem. Soc. 2010; 132:12214–12215. [PubMed: 20712312]
5. Kumar D, Thiel W, de Visser SP. J. Am. Chem. Soc. 2011; 133:3869–3882. [PubMed: 21344861]
6. Aluri S, de Visser SP. J. Am. Chem. Soc. 2007; 129:14846–14847. [PubMed: 17994747]
7. Simmons CR, Krishnamoorthy K, Granett SL, Schuller DJ, Dominy JE Jr, Begley TP, Stipanuk MH, Karplus PA. Biochemistry. 2008; 47:11390–11392. [PubMed: 18847220]
8. Ray K, Pfaff FF, Wang B, Nam W. J. Am. Chem. Soc. 2014; 136:13942–13958. [PubMed: 25215462]
9. Heafield MT, Fearn S, Steventon GB, Waring RH, Williams AC, Sturman SG. Neurosci. Lett. 1990; 110:216–220. [PubMed: 2325885]
10. Driggers, CM., Stipanuk, MH., Karplus, PA. Encyclopedia of Inorganic and Bioinorganic Chemistry. New York: John Wiley & Sons; 2015. Mammalian Cysteine Dioxygenase; p. 1-11. [Online] http://onlinelibrary.wiley.com/book/10.1002/9781119951438
11. Brait M, Ling S, Nagpal JK, Chang X, Park HL, Lee J, Okamura J, Yamashita K, Sidransky D, Kim MS. PLoS One. 2012; 7:e44951. [PubMed: 23028699]
12. Jeschke J, O'Hagan HM, Zhang W, Vatapalli R, Freitas Calmon M, Danilova L, Nelkenbrecher C, Van Neste L, Bijsmans IT, G W, Van Engeland M, Gabrielson E, Schuebel KE, Winterpacht A, Baylin SB, Herman JG, Ahuja N. Clin. Cancer Res. 2013; 19:3201–3211. [PubMed: 23630167]
13. Chiang C-W, Kleespies ST, Stout HD, Meier KK, Li P-Y, Bominaar EL, Que L Jr, Münck E, Lee W-Z. J. Am. Chem. Soc. 2014; 136:10846–10849. [PubMed: 25036460]
14. Hong S, Sutherlin KD, Park J, Kwon E, Siegler MA, Solomon EI, Nam W. Nat. Commun. 2014; 5:5440. [PubMed: 25510711]
15. Sahu S, Goldberg DP. J. Am. Chem. Soc. 2016; 138:11410–11428. [PubMed: 27576170]
16. Harrop TC, Mascharak PK. Acc. Chem. Res. 2004; 37:253–260. [PubMed: 15096062]
17. Lugo-Mas P, Taylor W, Schweitzer D, Theisen RM, Xu L, Shearer J, Swartz RD, Gleaves MC, DiPasquale A, Kaminsky W, Kovacs JA. Inorg. Chem. 2008; 47:11228–11236. [PubMed: 18989922]
18. Noveron JC, Olmstead MM, Mascharak PK. J. Am. Chem. Soc. 2001; 123:3247–3259. [PubMed: 11457060]
19. Tyler LA, Noveron JC, Olmstead MM, Mascharak PK. Inorg. Chem. 2000; 39:357–362. [PubMed: 11272547]
20. Heinrich L, Li Y, Vaissermann J, Chottard G, Chottard J-C. Angew. Chem., Int. Ed. 1999; 38:3526–3528.
21. Sallmann M, Siewert I, Fohlmeister L, Limberg C, Knispel C. Angew. Chem., Int. Ed. 2012; 51:2234–2237.
22. McQuilken AC, Goldberg DP. Dalton Trans. 2012; 41:10883–10899. [PubMed: 22814765]
23. Widger LR, Jiang Y, Siegler MA, Kumar D, Latifi R, de Visser SP, Jameson GNL, Goldberg DP. Inorg. Chem. 2013; 52:10467–10480. [PubMed: 23992096]
24. Grapperhaus CA, Darensbourg MY. Acc. Chem. Res. 1998; 31:451–459.
25. Leonard SE, Reddie KG, Carroll KS. ACS Chem. Biol. 2009; 4:783–799. [PubMed: 19645509]
26. Claiborne A, Yeh JI, Mallett TC, Luba J, Crane EJ, Charrier V, Parsonage D. Biochemistry. 1999; 38:15407–15416. [PubMed: 10569923]
27. Light KM, Yamanaka Y, Odaka M, Solomon EI. Chem. Sci. 2015; 6:6280–6294. [PubMed: 26508996]
28. Hashimoto K, Suzuki H, Taniguchi K, Noguchi T, Yohda M, Odaka M. J. Biol. Chem. 2008; 283:36617–36623. [PubMed: 18948265]
29. Murakami T, Nojiri M, Nakayama H, Odaka M, Yohda M, Dohmae N, Takio K, Nagamune T, Endo I. Protein Sci. 2000; 9:1024–1030. [PubMed: 10850812]

30. Nojiri M, Yohda M, Odaka M, Matsushita Y, Tsujimura M, Yoshida T, Dohmae N, Takio K, Endo I. J. Biochem. 1999; 125:696–704. [PubMed: 10101282]
31. Martinez S, Wu R, Sanishvili R, Liu D, Holz R. J. Am. Chem. Soc. 2014; 136:1186–1189. [PubMed: 24383915]
32. Yeh JI, Claiborne A, Hol WGI. Biochemistry. 1996; 35:9951–9957. [PubMed: 8756456]
33. Chae HZ, Robison K, Poole LB, Church G, Storz G, Rhee SG. Proc. Natl. Acad. Sci. U. S. A. 1994; 91:7017–7021. [PubMed: 8041738]
34. Mitra S, Holz RC. J. Biol. Chem. 2007; 282:7397–7404. [PubMed: 17150969]
35. Noguchi T, Nojiri M, Takei K, Odaka M, Kamiya N. Biochemistry. 2003; 42:11642–11650. [PubMed: 14529274]
36. Kobayashi M, Shimizu S. Nat. Biotechnol. 1998; 16:733–736. [PubMed: 9702770]
37. Sugiura Y, Kuwahara J, Nagasawa T, Yamada H. J. Am. Chem. Soc. 1987; 109:5848–5850.
38. Stolz A, Trott S, Binder M, Bauer R, Hirrlinger B, Layh N, Knackmuss H-J. J. Mol. Catal. B: Enzym. 1998; 5:137–141.
39. Dey A, Chow M, Taniguchi K, Lugo-Mas P, Davin SD, Maeda M, Kovacs JA, Odaka M, Hedman B, Hodgson KO, Solomon EI. J. Am. Chem. Soc. 2006; 128:533–541. [PubMed: 16402841]
40. Song L, Wang M, Shi J, Xue Z, Wang M-X, Qian S. Biochem. Biophys. Res. Commun. 2007; 362:319–324. [PubMed: 17716629]
41. Nagashima S, Nakasako M, Dohmae N, Tsujimura M, Takio K, Odaka M, Yohda M, Kamiya N, Endo I. Nat. Struct. Biol. 1998; 5:347–351. [PubMed: 9586994]
42. Tsujimura M, Odaka M, Nakayama H, Dohmae N, Koshino H, Asami T, Hoshino M, Takio K, Yoshida S, Maeda M, Endo I. J. Am. Chem. Soc. 2003; 125:11532. [PubMed: 13129355]
43. Yamanaka Y, Kato Y, Hashimoto K, Iida K, Nagasawa K, Nakayama H, Dohmae N, Noguchi K, Noguchi T, Yohda M, Odaka M. Angew. Chem., Int. Ed. 2015; 54:10763–10767.
44. Goto K, Holler M, Okazaki R. J. Am. Chem. Soc. 1997; 119:1460–1461.
45. Allison WS. Acc. Chem. Res. 1976; 9:293–299.
46. Adzamli IK, Libson K, Lydon JD, Elder RC, Deutsch E. Inorg. Chem. 1979; 18:303–311.
47. Bachi MD, Gross A. J. Org. Chem. 1982; 47:897–898.
48. Lugo-Mas P, Dey A, Xu L, Davin SD, Benedict J, Kaminsky W, Hodgson KO, Hedman B, Solomon EI, Kovacs JA. J. Am. Chem. Soc. 2006; 128:11211–11221. [PubMed: 16925440]
49. Kung IY, Schweitzer D, Shearer J, Taylor WD, Jackson HL, Lovell S, Kovacs JA. J. Am. Chem. Soc. 2000; 122:8299–8300.
50. Coggins MK, Sun X, Kwak Y, Solomon EI, Rybak-Akimova EV, Kovacs JA. J. Am. Chem. Soc. 2013; 135:5631–5640. [PubMed: 23470101]
51. Theisen RM, Shearer J, Kaminsky W, Kovacs JA. Inorg. Chem. 2004; 43:7682–7690. [PubMed: 15554633]
52. Kovacs JA. Science. 2003; 299:1024–1025. [PubMed: 12586930]
53. Kitagawa T, Dey A, Lugo-Mas P, Benedict J, Kaminsky W, Solomon E, Kovacs JA. J. Am. Chem. Soc. 2006; 128:14448–14449. [PubMed: 17090014]
54. Shearer J, Scarrow RC, Kovacs JA. J. Am. Chem. Soc. 2002; 124:11709–11717. [PubMed: 12296737]
55. Kovacs JA. Acc. Chem. Res. 2015; 48:2744–2753. [PubMed: 26335158]
56. Coggins MK, Martin-Diaconescu V, De Beer S, Kovacs JA. J. Am. Chem. Soc. 2013; 135:4260–4272. [PubMed: 23432090]
57. Coggins MK, Brines LM, Kovacs JA. Inorg. Chem. 2013; 52:12383–12393. [PubMed: 24156315]
58. Coggins MK, Kovacs JA. J. Am. Chem. Soc. 2011; 133:12470–12473. [PubMed: 21776951]
59. Kovacs JA, Brines LM. Acc. Chem. Res. 2007; 40:501–509. [PubMed: 17536780]
60. Kovacs JA. Chem. Rev. 2004; 104:825–848. [PubMed: 14871143]
61. Schweitzer D, Shearer J, Rittenberg DK, Shoner SC, Ellison JJ, Loloee R, Lovell SC, Barnhart D, Kovacs JA. Inorg. Chem. 2002; 41:3128–3136. [PubMed: 12054991]
62. Shoner SC, Nienstedt A, Ellison JJ, Kung I, Barnhart D, Kovacs JA. Inorg. Chem. 1998; 37:5721–5725.

63. Ellison JJ, Nienstedt A, Shoner SC, Barnhart D, Cowen JA, Kovacs JA. J. Am. Chem. Soc. 1998; 120:5691–5700.
64. Shearer J, Nehring J, Lovell S, Kaminsky W, Kovacs JA. Inorg. Chem. 2001; 40:5483–5484. [PubMed: 11599942]
65. Shearer J, Fitch SB, Kaminsky W, Benedict J, Scarrow RC, Kovacs JA. Proc. Natl. Acad. Sci. U. S. A. 2003; 100:3671–3676. [PubMed: 12655068]
66. Shearer J, Jackson HL, Schweitzer D, Rittenberg DK, Leavy TM, Kaminsky W, Scarrow RC, Kovacs JA. J. Am. Chem. Soc. 2002; 124:11417–11428. [PubMed: 12236756]
67. Theisen R, Shearer J, Kaminsky W, Kovacs J. Inorg. Chem. 2004; 43:7682–7690. [PubMed: 15554633]
68. Grapperhaus CA, Li M, Patra AK, Poturovic S, Kozlowski PM, Zgierski MZ, Mashuta MS. Inorg. Chem. 2003; 42:4382–4388. [PubMed: 12844310]
69. Namuswe F, Kasper GD, Sarjeant AAN, Hayashi T, Krest CM, Green MT, Moenne-Loccoz P, Goldberg DP. J. Am. Chem. Soc. 2008; 130:14189–14200. [PubMed: 18837497]
70. Jiang Y, Telser J, Goldberg DP. Chem. Commun. 2009:6828–6830.
71. Shearer J, Nehring J, Lovell S, Kaminsky W, Kovacs J. Inorg. Chem. 2001; 40:5483–5484. [PubMed: 11599942]
72. Brines LM, Shearer J, Fender JK, Schweitzer D, Shoner SC, Barnhart D, Kaminsky W, Lovell S, Kovacs JA. Inorg. Chem. 2007; 46:9267–9277. [PubMed: 17867686]
73. Brines LM, Villar-Acevedo G, Kitagawa T, Swartz RD, Lugo-Mas P, Kaminsky W, Benedict JB, Kovacs JA. Inorg. Chim. Acta. 2008; 361:1070–1078.
74. Shearer J, Kung I, Lovell S, Kovacs JA. Inorg. Chem. 2000; 39:4998–4999. [PubMed: 11233193]
75. Theisen RM, Kovacs JA. Inorg. Chem. 2005; 44:1169–1171. [PubMed: 15732947]
76. Villar-Acevedo G, Nam E, Fitch S, Benedict J, Freudenthal J, Kaminsky W, Kovacs JA. J. Am. Chem. Soc. 2011; 133:1419–1427. [PubMed: 21207999]
77. Nam E, Alokolaro PE, Swartz RD, Gleaves MC, Pikul J, Kovacs JA. Inorg. Chem. 2011; 50:1592–1602. [PubMed: 21284379]
78. Schweitzer D, Ellison JJ, Shoner SC, Lovell S, Kovacs JA. J. Am. Chem. Soc. 1998; 120:10996–10997.
79. Kennepohl P, Neese F, Schweitzer D, Jackson HL, Kovacs JA, Solomon EI. Inorg. Chem. 2005; 44:1826–1836. [PubMed: 15762709]
80. Shearer J, Kung IY, Lovell S, Kaminsky W, Kovacs JA. J. Am. Chem. Soc. 2001; 123:463–468. [PubMed: 11456548]
81. Live DH, Chan SI. Anal. Chem. 1970; 42:791.
82. Evans DA. J. Chem. Soc. 1959:2003–2005.
83. Van Geet AL. Anal. Chem. 1968; 40:2227–2229.
84. Neese F. Interdiscip. Rev. Comput. Mol. Sci. 2012; 2:73–78.
85. Becke AD. Phys. Rev. A: At., Mol., Opt. Phys. 1988; 38:3098–3100.
86. Perdew JP. Phys. Rev. B: Condens. Matter Mater. Phys. 1986; 33:8822–8224.
87. Weigend F. Phys. Chem. Chem. Phys. 2006; 8:1057–1065. [PubMed: 16633586]
88. Grimme S, Ehrlich S, Goerigk L. J. Comput. Chem. 2011; 32:1456–1465. [PubMed: 21370243]
89. Lenthe EV, Avoird AVD, Wormer PES. J. Chem. Phys. 1998; 108:4783–4796.
90. Weigend F, Ahlrichs R. Phys. Chem. Chem. Phys. 2005; 7:3297–3305. [PubMed: 16240044]
91. Klamt A, Schüürmann GJ. Chem. Soc., Perkin Trans. 2. 1993; 5:799–805.
92. Waasmaier D, Kirfel A. Acta Crystallogr., Sect. A: Found. Crystallogr. 1995; 51:416.
93. de Oliveira FT, Chanda A, Banerjee D, Shan X, Mondal S, Que L Jr, Bominaar EL, Münck E, Collins TJ. Science. 2007; 315:835–838. [PubMed: 17185561]
94. Lyakin OY, Zima AM, Samsonenko DG, Bryliakov KP, Talsi EP. ACS Catal. 2015; 5:2702–2707.
95. Ghosh M, Singh KK, Panda C, Weitz A, Hendrich MP, Collins TJ, Dhar BB, Gupta SS. J. Am. Chem. Soc. 2014; 136:9524–9527. [PubMed: 24387595]

96. Van Heuvelen KM, Fiedler AT, Shan X, De Hont RF, Meier KK, Bominaar EL, Münck E, Que L Jr. Proc. Natl. Acad. Sci. U. S. A. 2012; 109:11933–11938. [PubMed: 22786933]
97. Jackson HL, Shoner SC, Rittenberg D, Cowen JA, Lovell S, Barnhart D, Kovacs JA. Inorg. Chem. 2001; 40:1646–1653. [PubMed: 11261975]
98. Que L Jr. Acc. Chem. Res. 2007; 40:493–500. [PubMed: 17595051]
99. Rohde J-U, In JH, Lim MH, Brennessel WW, Bukowski MR, Stubna A, Münck E, Nam W, Que L Jr. Science. 2003; 299:1037–1039. [PubMed: 12586936]
100. Sastri CV, Park MJ, Ohta T, Jackson TA, Stubna A, Seo MS, Lee J, Kim J, Kitagawa T, Münck E, Que L Jr, Nam W. J. Am. Chem. Soc. 2005; 127:12494–12495. [PubMed: 16144389]
101. Nam W, Jin SW, Lim MH, Ryu JY, Kim C. Inorg. Chem. 2002; 41:3647–3652. [PubMed: 12099867]
102. Nam W, Choi SK, Lim MH, Rohde J-U, Kim I, Kim J, Kim C, Que L Jr. Angew. Chem., Int. Ed. 2003; 42:109–111.
103. Groves JT, Watanabe YJ. Am. Chem. Soc. 1988; 110:8443–8452.
104. Kundu S, Thompson JVK, Ryabov AD, Collins TJ. J. Am. Chem. Soc. 2011; 133:18546–18549. [PubMed: 21985217]
105. Meunier B, de Visser SP, Shaik S. Chem. Rev. 2004; 104:3947–3980. [PubMed: 15352783]
106. Rittle J, Green MT. Science. 2010; 330:933–937. [PubMed: 21071661]
107. Krest CM, Onderko EL, Yosca TH, Calixto JC, Karp RF, Livada J, Rittle J, Green MT. J. Biol. Chem. 2013; 288:17074–17081. [PubMed: 23632017]
108. Wang X, Peter S, Kinne M, Hofrichter M, Groves JT. J. Am. Chem. Soc. 2012; 134:12897–12900. [PubMed: 22827262]
109. Chreifi G, Baxter EL, Doukov T, Cohen AE, McPhillips SE, Song J, Meharenna YT, Soltis SM, Poulos TL. Proc. Natl. Acad. Sci. U. S. A. 2016; 113:1226–1231. [PubMed: 26787871]
110. Barrows TP, Poulos TL. Biochemistry. 2005; 44:14062–14068. [PubMed: 16245922]
111. Denisov IG, Makris TM, Sligar SG, Schlichting I. Chem. Rev. 2005; 105:2253–2277. [PubMed: 15941214]
112. Oloo WN, Que L Jr. Acc. Chem. Res. 2015; 48:2612–2621. [PubMed: 26280131]
113. Prat E, Mathieson JS, Güell M, Ribas X, Luis JM, Cronin L, Costas M. Nat. Chem. 2011; 3:788–793. [PubMed: 21941251]
114. Decker A, Rohde J-U, Klinker RJ, Wong SD, Que L Jr, Solomon EI. J. Am. Chem. Soc. 2007; 129:15983–15996. [PubMed: 18052249]
115. Bukowski MR, Koehntop KD, Stubna A, Bominaar EL, Halfen JA, Münck E, Nam W, Que L. Science. 2005; 310:1000–1002. [PubMed: 16254150]
116. Costas M, Mehn MP, Jensen MP, Que L Jr. Chem. Rev. 2004; 104:939–986. [PubMed: 14871146]
117. Puri M, Que L Jr. Acc. Chem. Res. 2015; 48:2443–2452. [PubMed: 26176555]
118. Sahu S, Quesne MG, Davies CG, Dürr M, Ivanović-Burmazovic I, Siegler MA, Jameson GNL, de Visser SP, Goldberg DP. J. Am. Chem. Soc. 2014; 136:13542–13545. [PubMed: 25246108]
119. Lacy DC, Gupta R, Stone KL, Greaves J, Ziller JW, Hendrich MP, Borovik AS. J. Am. Chem. Soc. 2010; 132:12188–12190. [PubMed: 20704272]
120. Solomon EI, Wong SD, Liu LV, Decker A, Chow MS. Curr. Opin. Chem. Biol. 2009; 13:99–113. [PubMed: 19278895]
121. Nam W. Acc. Chem. Res. 2015; 48:2415–2423. [PubMed: 26203519]
122. Thibon A, England J, Martinho M, Young VG Jr, Frisch JR, Guillot R, Girerd J-J, Münck E, Que L Jr, Banse F. Angew. Chem., Int. Ed. 2008; 47:7064–7067.
123. Hohenberger J, Ray K, Meyer K. Nat. Commun. 2012; 3:720. [PubMed: 22395611]
124. McDonald AR, Que L Jr. Nat. Chem. 2011; 3:761–762. [PubMed: 21941247]
125. Kundu S, Thompson JVK, Shen LQ, Mills MR, Bominaar EL, Ryabov AD, Collins TJ. Chem. - Eur. J. 2015; 21:1803–1810. [PubMed: 25410933]
126. Panda C, Debgupta J, Díaz Díaz D, Singh KK, Sen Gupta S, Dhar BB. J. Am. Chem. Soc. 2014; 136:12273–12282. [PubMed: 25119524]

127. Groves JT, Haushalter RC, Nakamura M, Nemo TE, Evans BJ. J. Am. Chem. Soc. 1981; 103:2884–2886.
128. Buonomo RM, Font I, Maguire MJ, Reibenspies JH, Tuntulani T, Darensbourg MY. J. Am. Chem. Soc. 1995; 117:963–973.
129. Heinrich L, Mary-Verla A, Li Y, Vaissermann J, Chottard JC. Eur. J. Inorg. Chem. 2001; 2001:2203–2206.
130. Lydon JD, Deutsch E. Inorg. Chem. 1982; 21:3180–3185.
131. Cornman CR, Stauffer TC, Boyle PD. J. Am. Chem. Soc. 1997; 119:5986–5987.
132. Ge W, Clifton IJ, Stok JE, Adlington RM, Baldwin JE, Rutledge PJ. J. Am. Chem. Soc. 2008; 130:10096–10102. [PubMed: 18620394]
133. Noveron JC, Olmstead MM, Mascharak PK. Inorg. Chem. 1998; 37:1138–1139. [PubMed: 11670316]
134. Costas M, Harvey JN. Nat. Chem. 2013; 5:7–9. [PubMed: 23247168]
135. Carreon-Macedo J-L, Harvey JN. J. Am. Chem. Soc. 2004; 126:5789–5797. [PubMed: 15125671]
136. Shoner S, Barnhart D, Kovacs JA. Inorg. Chem. 1995; 34:4517–4518.
137. Ye W, Ho DM, Friedle S, Palluccio TD, Rybak-Akimova EV. Inorg. Chem. 2012; 51:5006–5021. [PubMed: 22534174]
138. Lennartson A, McKenzie CJ. Angew. Chem., Int. Ed. 2012; 51:6767–6770.
139. Hong S, Wang B, Seo MS, Lee YM, Kim MJ, Kim HR, Ogura T, Garcia-Serres R, Clémancey M, Latour JM, Nam W. Angew. Chem., Int. Ed. 2014; 53:6388–6392.
140. Wang C, Kurahashi T, Inomata K, Hada M, Fujii H. Inorg. Chem. 2013; 52:9557–9566. [PubMed: 23909819]
141. Wang SH, Mandimutsira BS, Todd R, Ramdhanie B, Fox JP, Goldberg DP. J. Am. Chem. Soc. 2004; 126:18–19. [PubMed: 14709038]
142. Yang Y, Diederich F, Valentine JS. J. Am. Chem. Soc. 1990; 112:7826–7828.

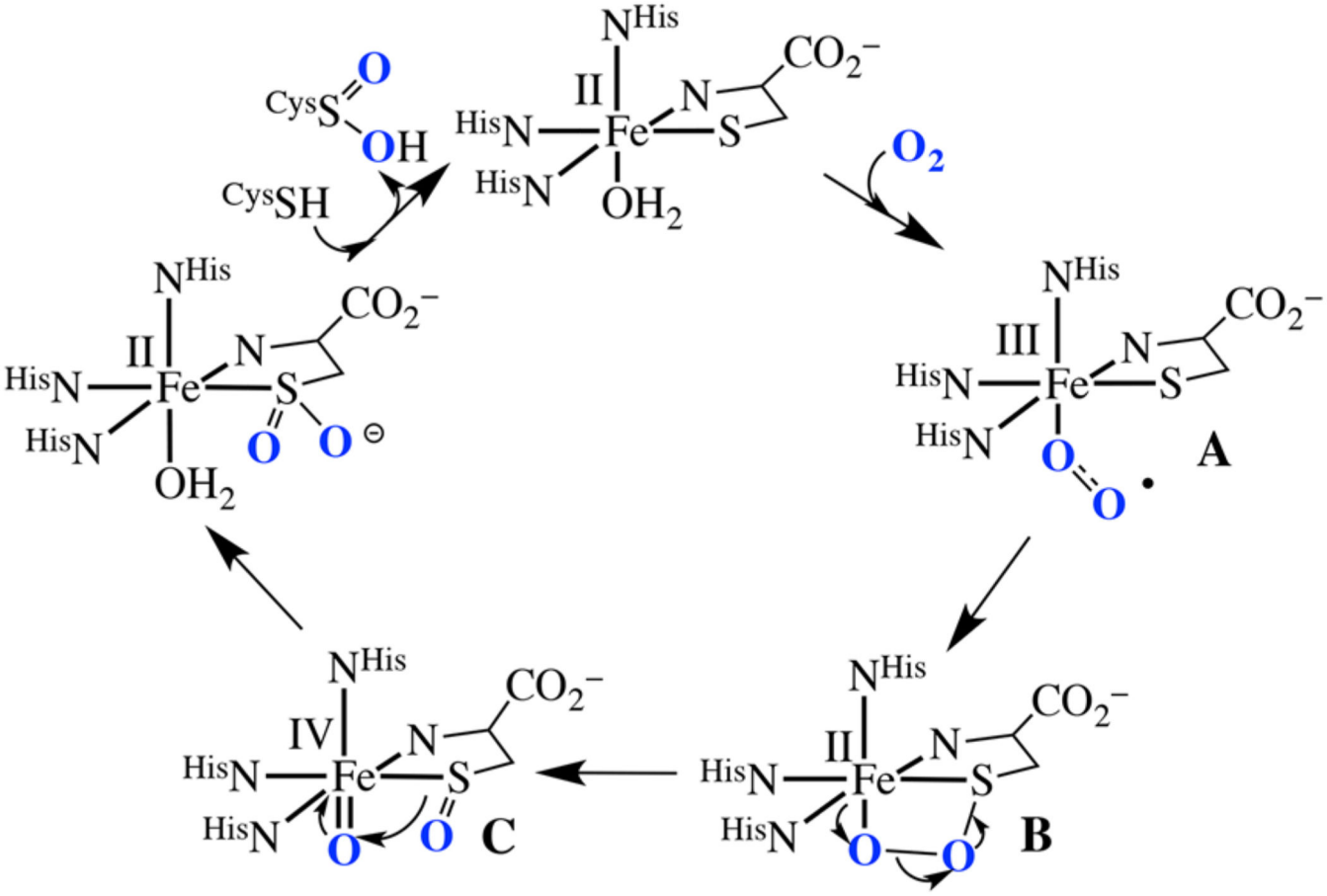

Figure 1.
Proposed mechanism of CDO catalyzed cysteine oxygenation.

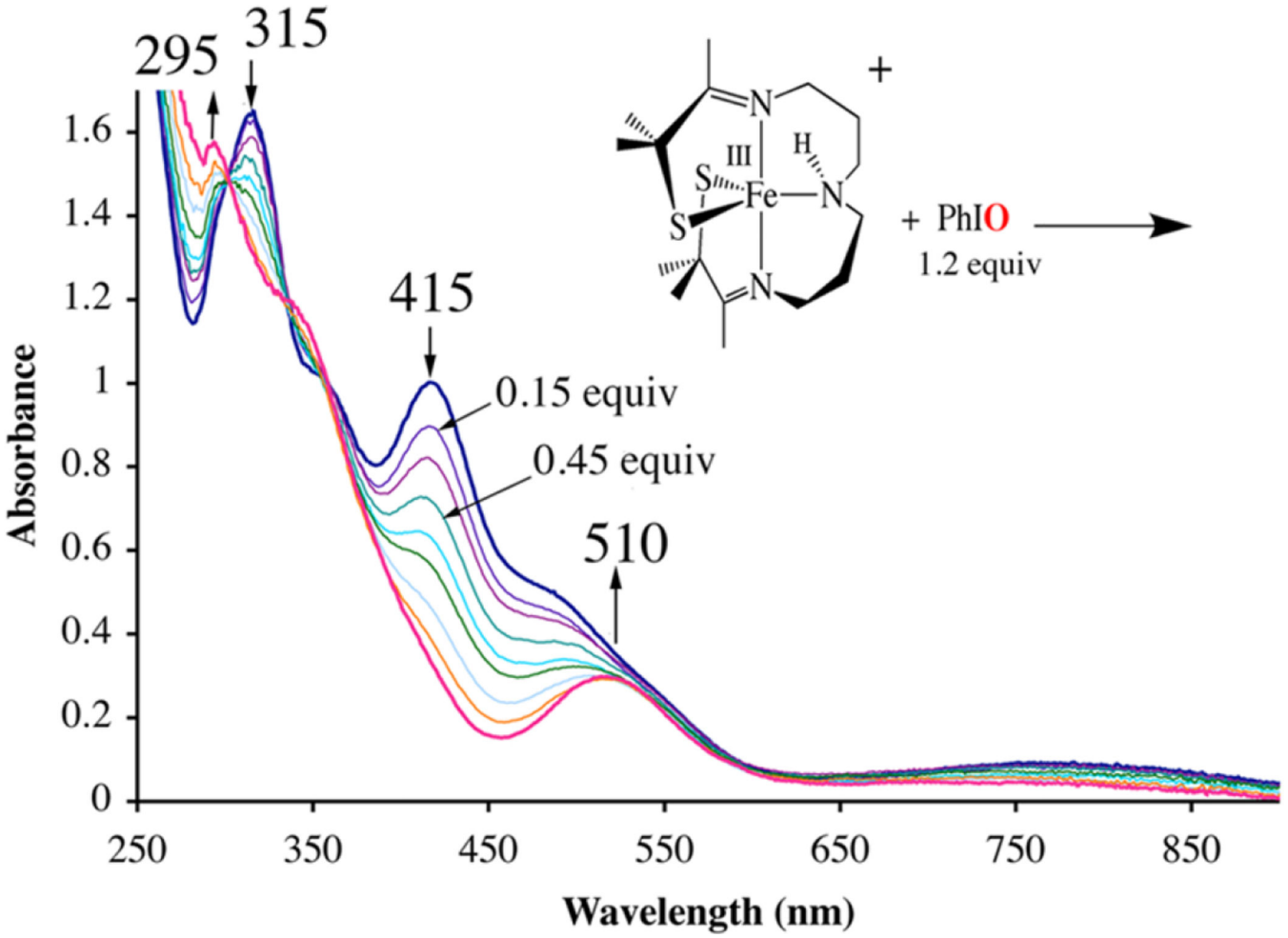

Figure 2.

Use of electronic absorption spectroscopy to monitor the reaction between $[Fe^{III}(S_2{}^{Me2}N_3(Pr,Pr))]^+$ (**2**) and 1.2 equiv of PhIO, added in 0.15 equiv aliquots, in MeOH at 298 K.

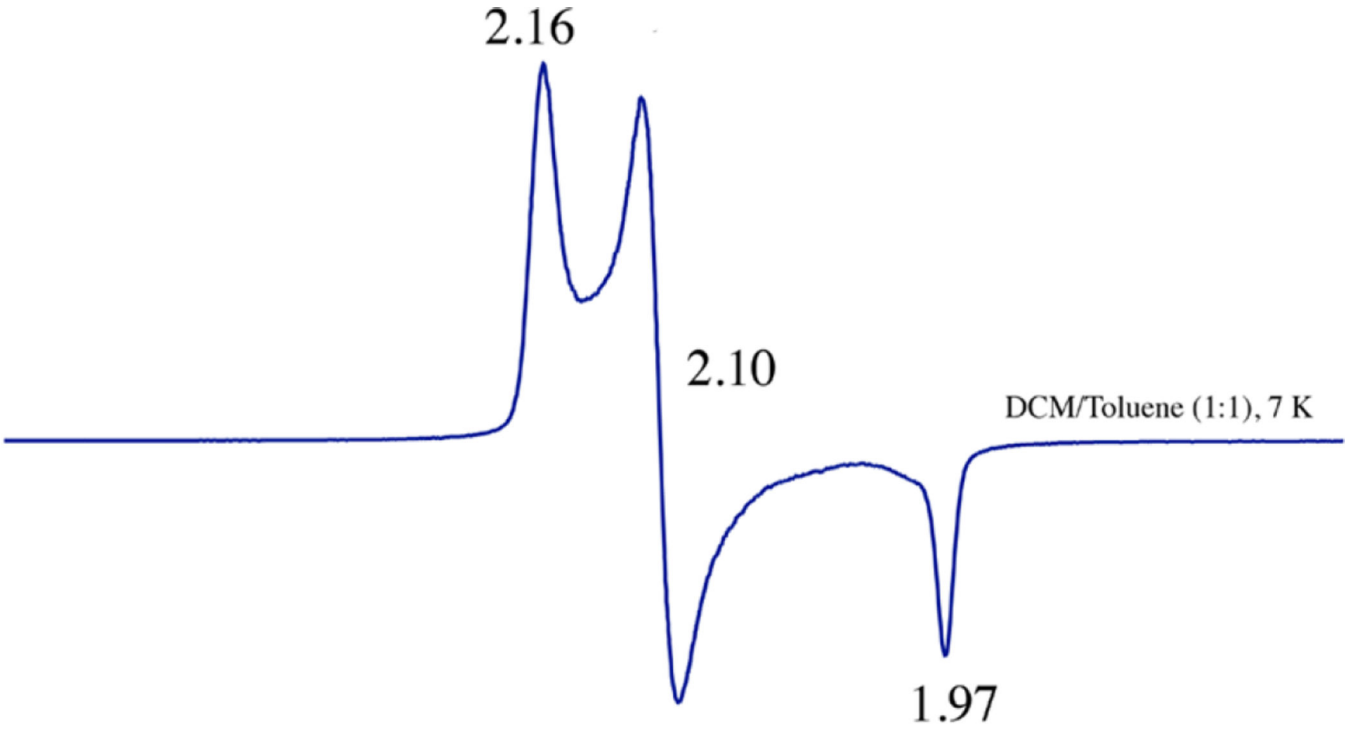

Figure 3.
Low-temperature (7 K) X-band EPR spectrum of **5** in CH_2Cl_2/toluene (1:1) glass.

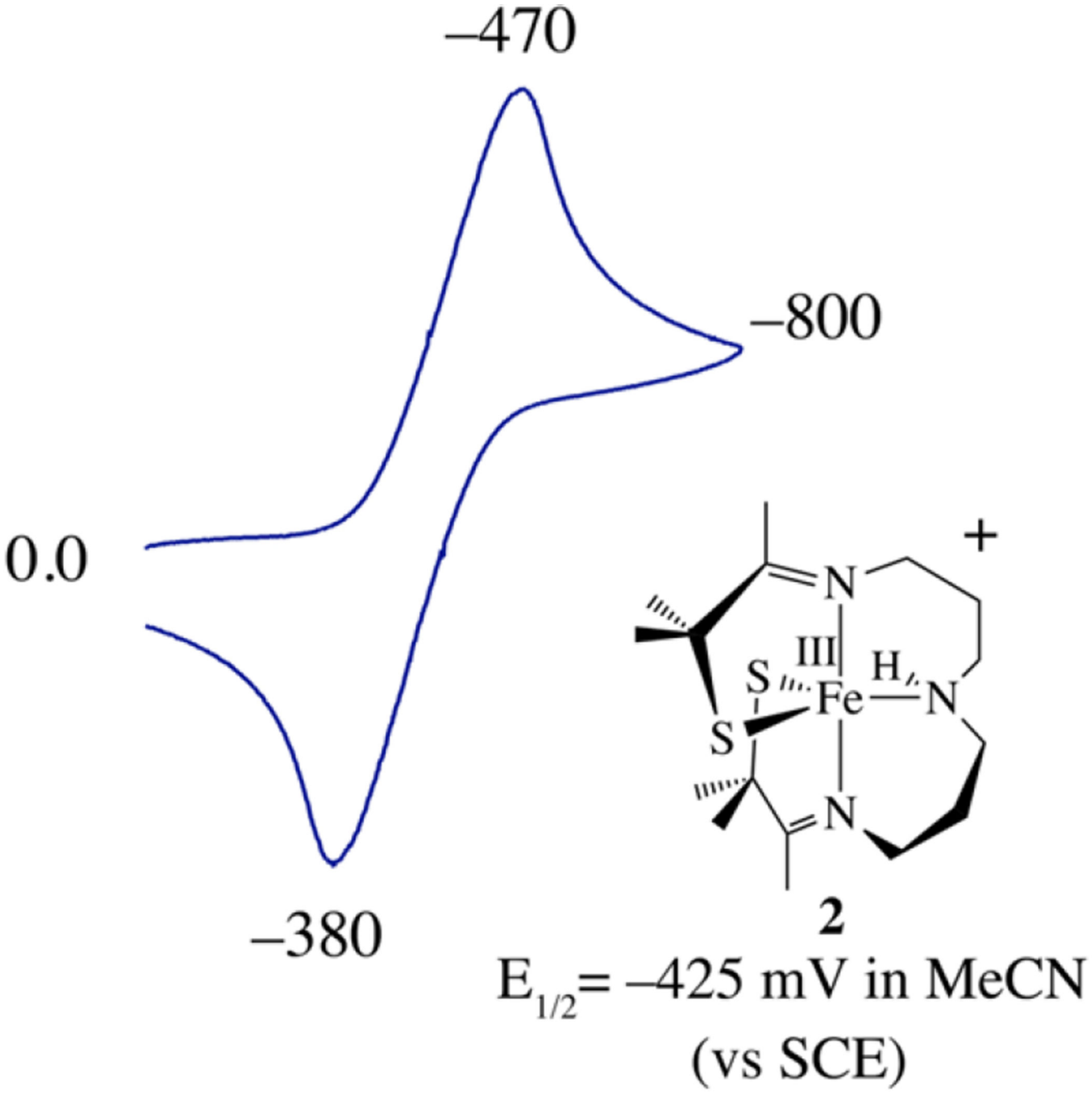

Figure 4.

Cyclic voltammogram of five-coordinate $[Fe^{III}(S_2{}^{Me2}N_3\text{-}(Pr,Pr))]^+$ (**2**) in MeCN at 298 K (0.1 M $(Bu_4N)PF_6$, glassy carbon electrode, 150 mV/s scan rate). Peak potentials versus SCE are indicated.

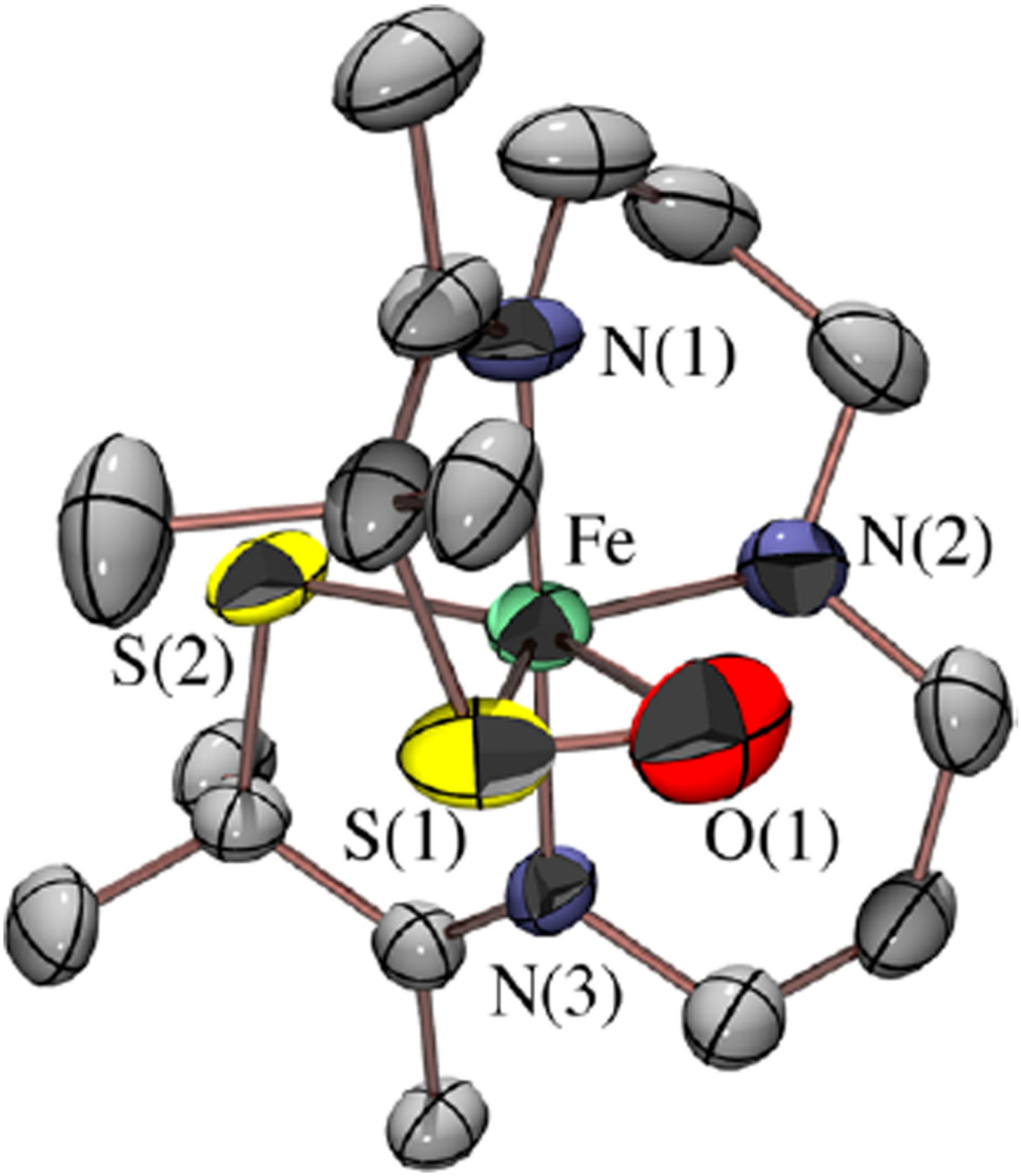

Figure 5.

ORTEP diagram of the cation of $[Fe^{III}(\eta^2\text{-}S^{Me2}O)(S^{Me2})\text{-}N_3(Pr,Pr)](PF_6)$ (**5**) showing the atom labeling scheme. The anion, and all hydrogen atoms have been removed for clarity.

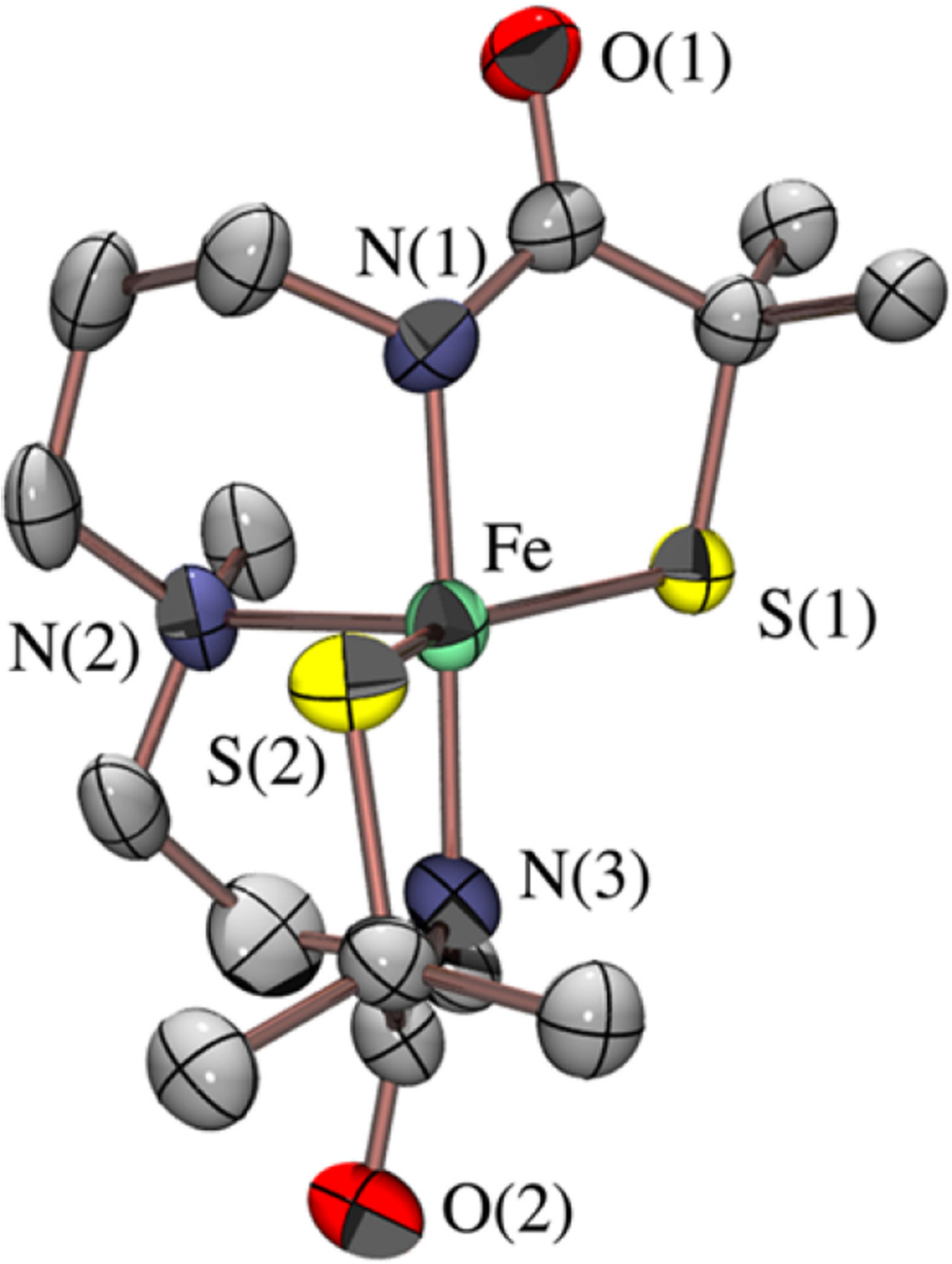

Figure 6.

ORTEP diagram of the anion of $(Et_4N)[Fe^{III}\text{-}S_2{}^{Me2}N^{Me}N_2{}^{amide}(Pr,Pr)]$ (**8**), showing the atom labeling scheme. The cation, and all hydrogen atoms have been removed for clarity.

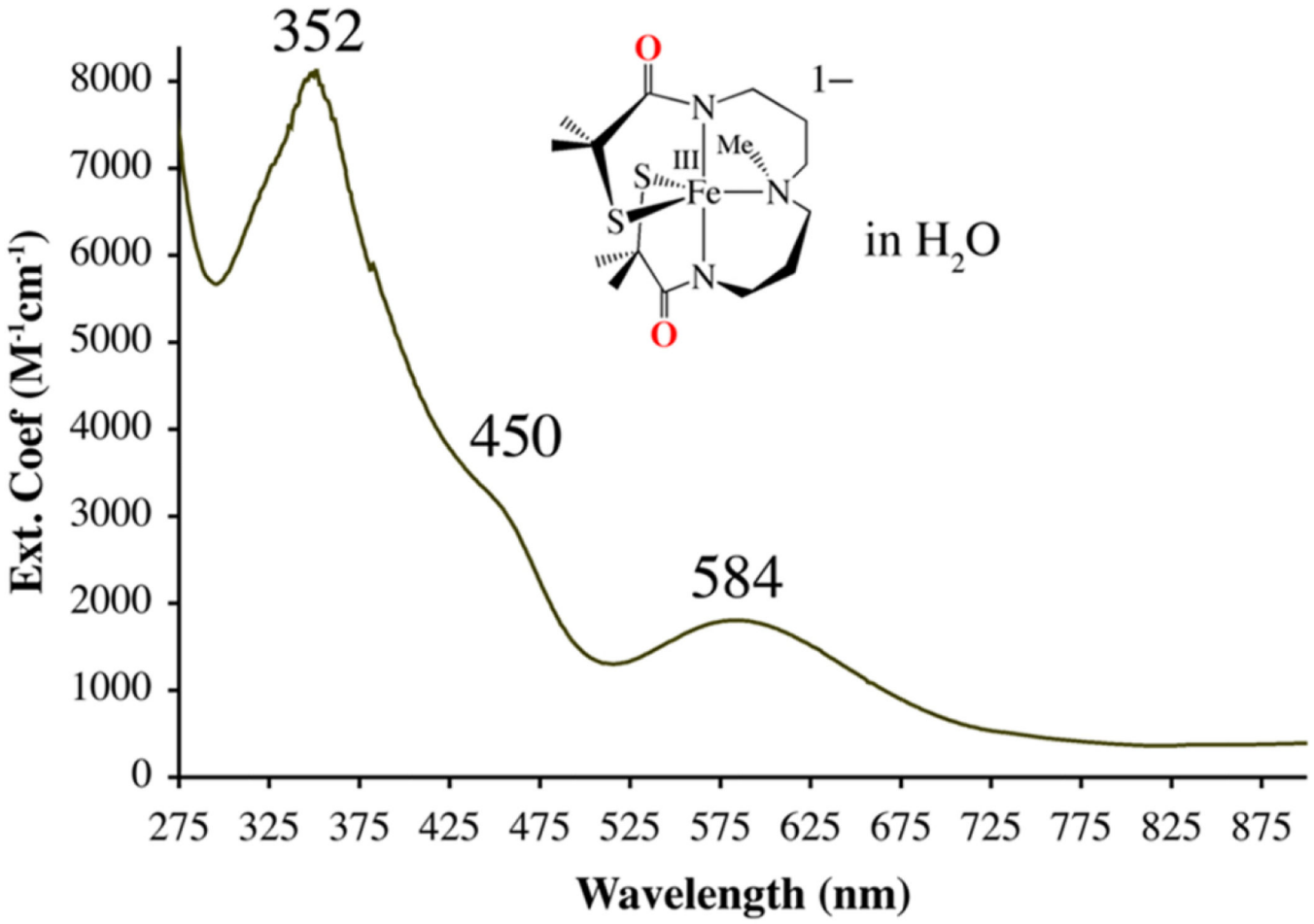

Figure 7.

Electronic absorption spectrum of $(Et_4N)[Fe^{III}\text{-}S_2{}^{Me2}N^{Me}N_2{}^{amide}(Pr,Pr)]$ (**8**) in H_2O at 298 K.

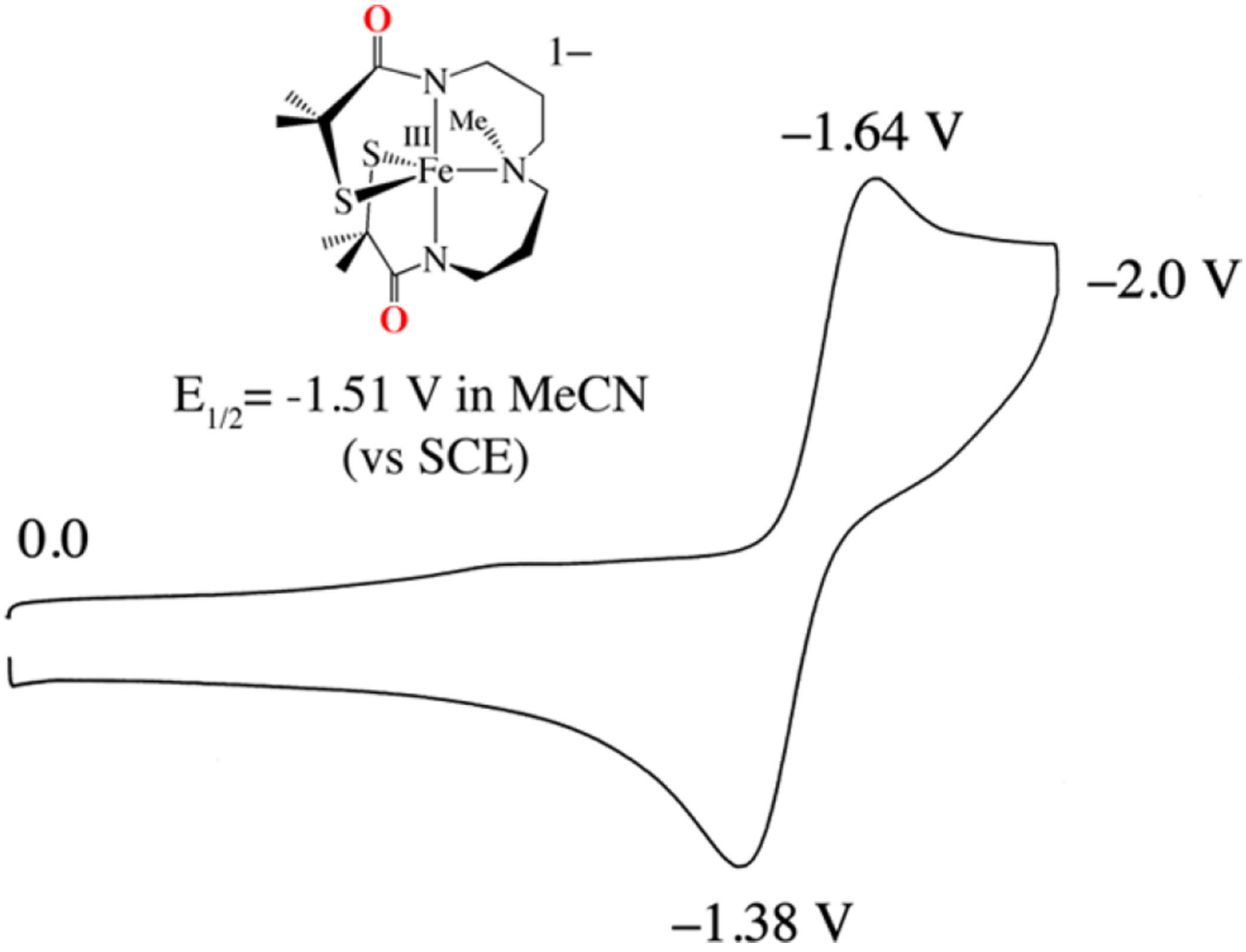

Figure 8.

Cyclic voltammogram of $(Et_4N)[Fe^{III}S_2{}^{Me2}N^{Me}N_2{}^{amide}$-(Pr,Pr)] (**8**) in MeCN at 298 K (0.1 M $(Bu_4N)PF_6$, glassy carbon electrode, 150 mV/s scan rate). Peak potentials versus SCE are indicated.

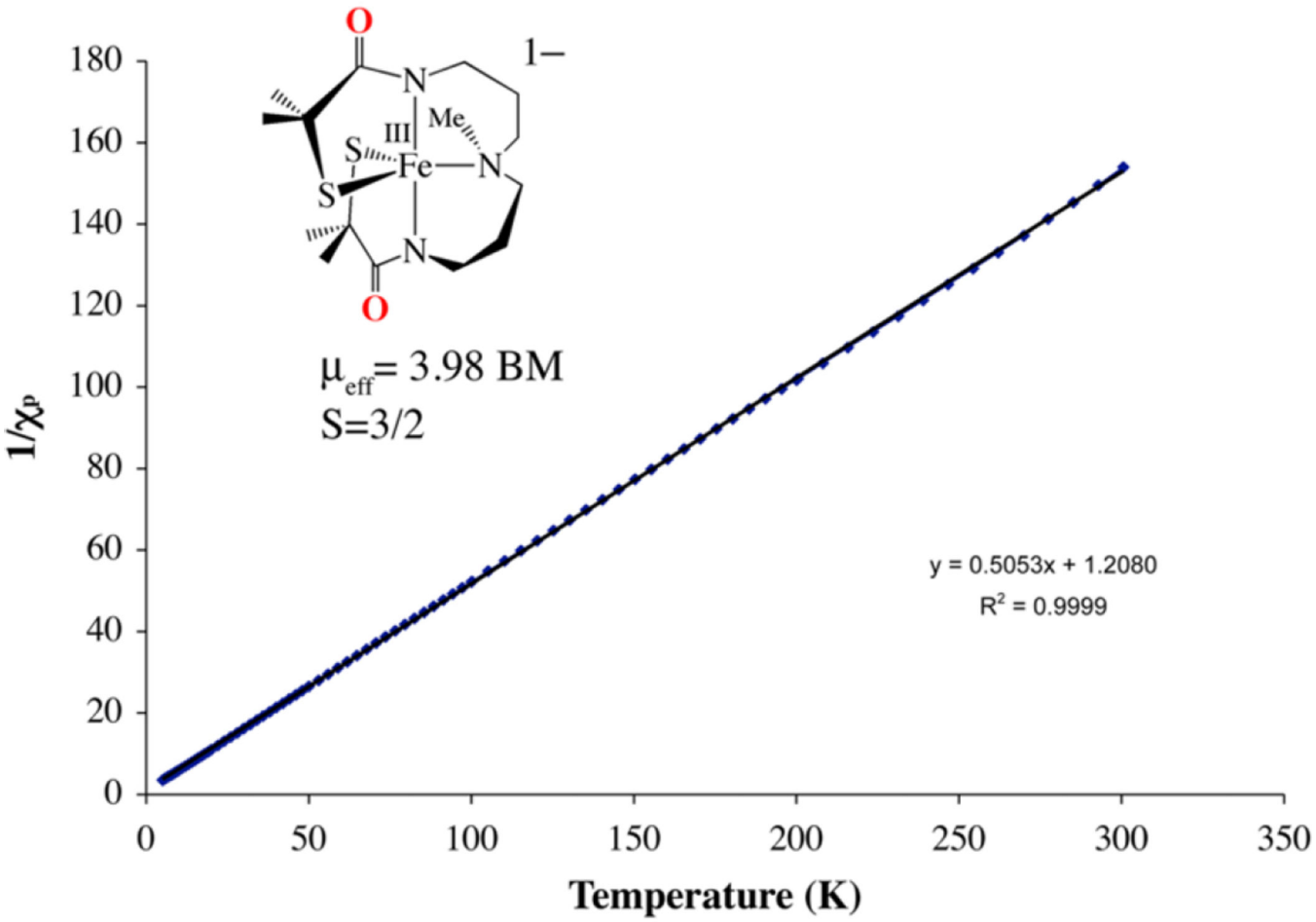

Figure 9.

Inverse molar magnetic susceptibility ($1/\chi_m$) vs temperature (*T*) plot for (Et_4N)[$Fe^{III}S_2{}^{Me2}N^{Me}N_2{}^{amide}$(Pr,Pr)] (**8**), fit to an $S = 3/2$ spin state.

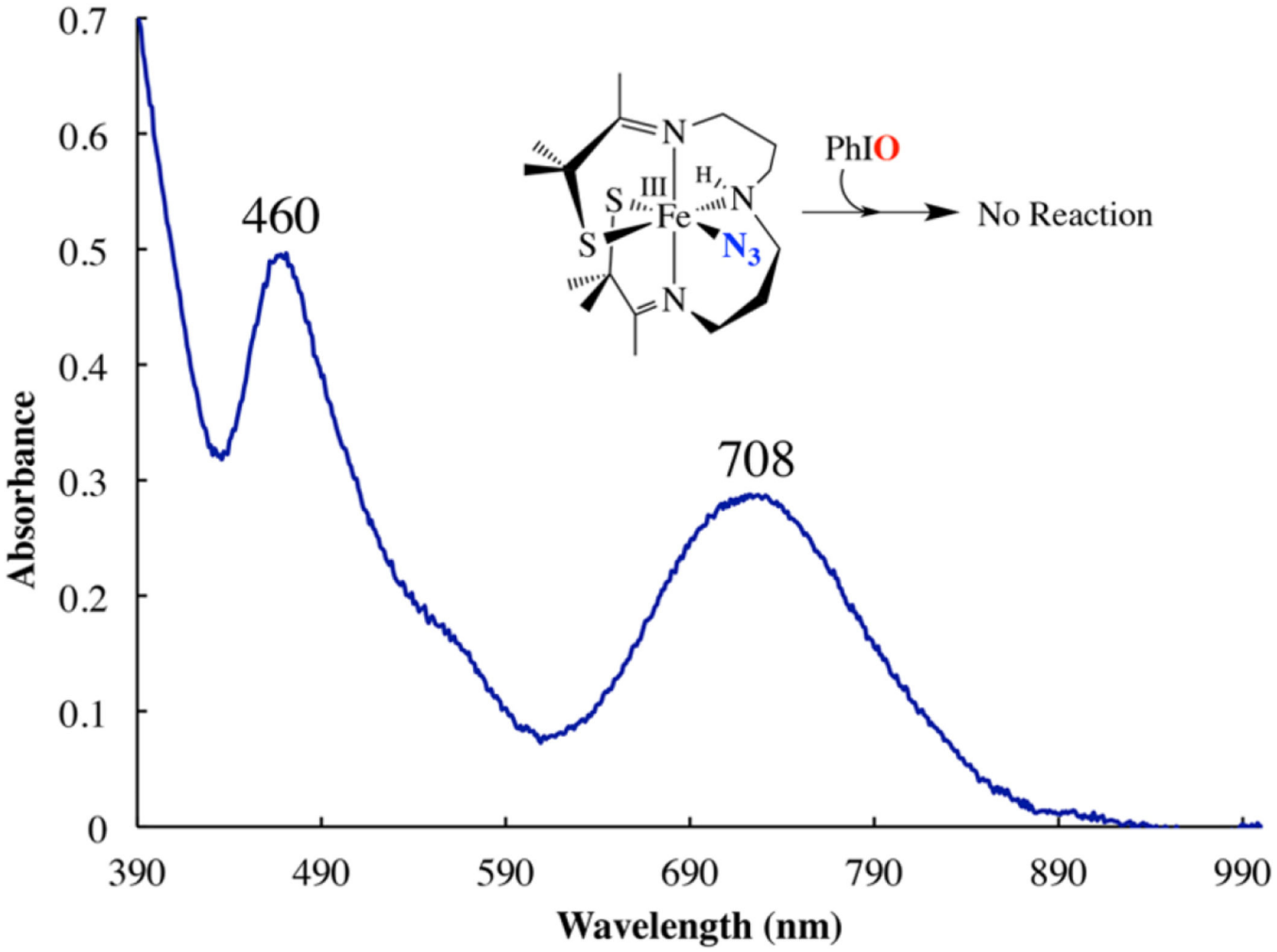

Figure 10.

Monitoring the addition of iodosylbenzene (PhIO) to [$Fe^{III}(S_2{}^{Me2}N_3(Pr,Pr))N_3$] (**4**) in MeOH at −73 °C via electronic absorption spectroscopy, showing that no reaction occurs.

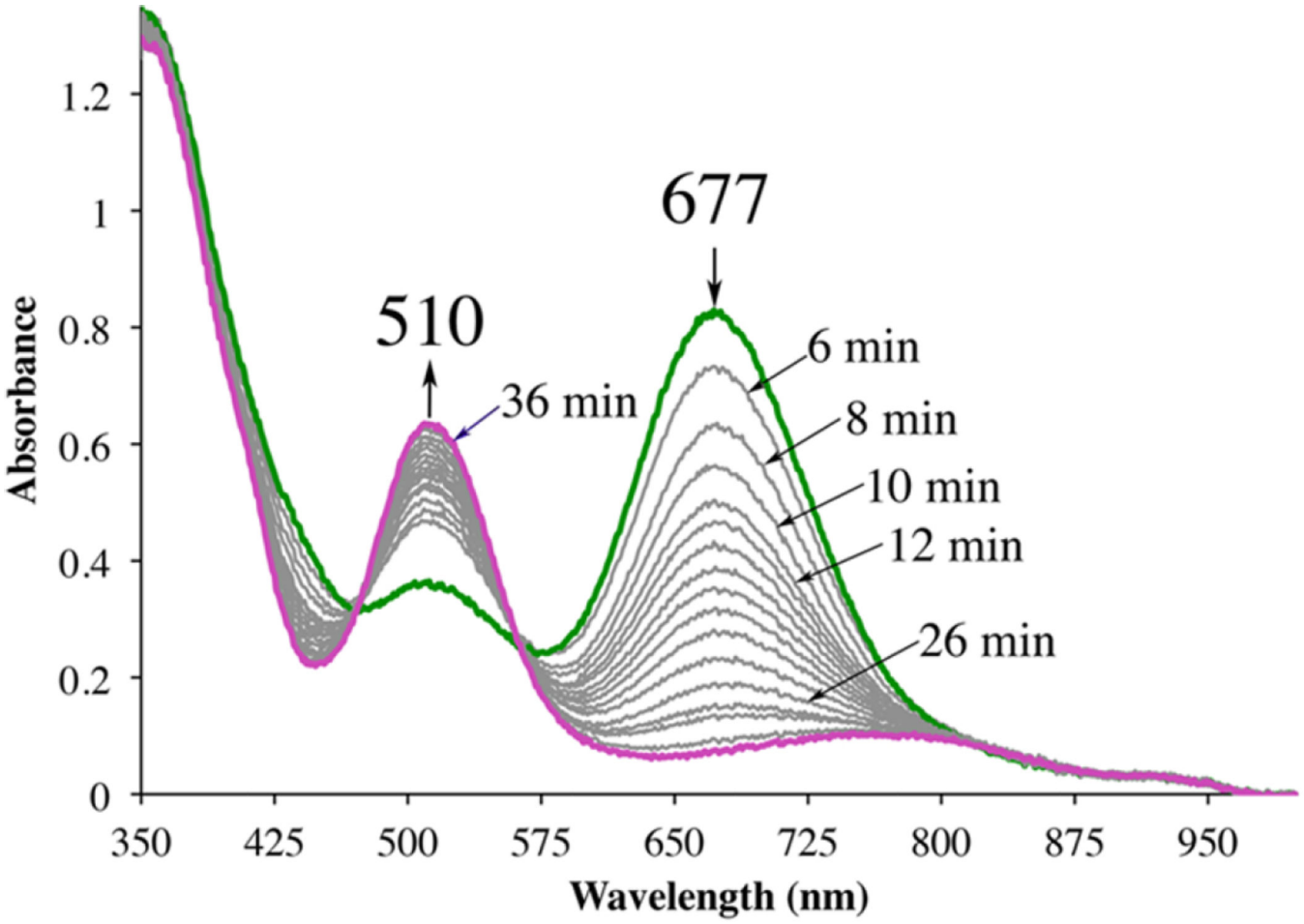

Figure 11.

Detection of a green metastable intermediate in the reaction between (Pr,Pr)Fe(III) (**2**) and 10 equiv of IBX-ester at −73 °C in MeOH to form sulfenate **5** over the course of 36 min.

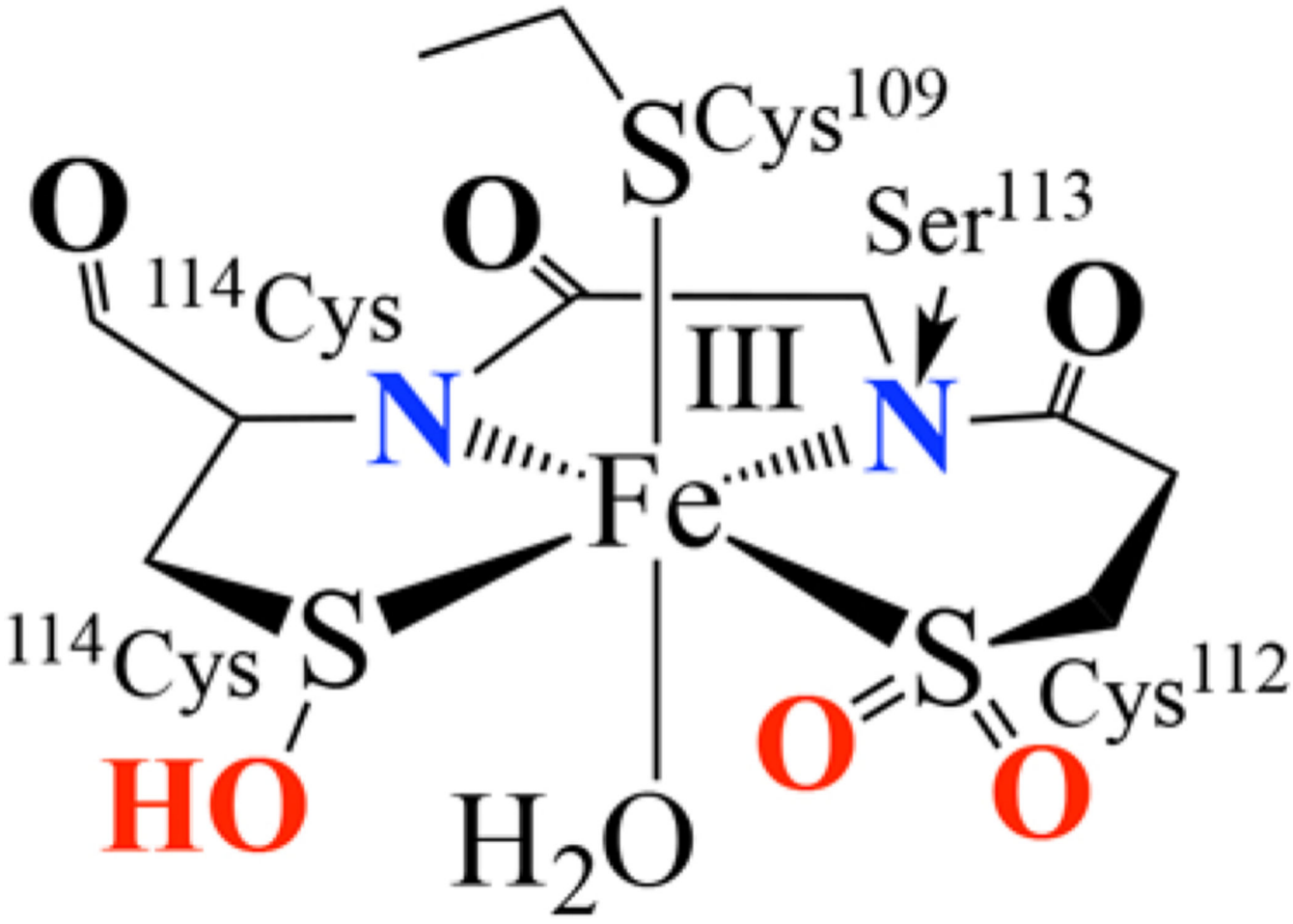

Scheme 1.

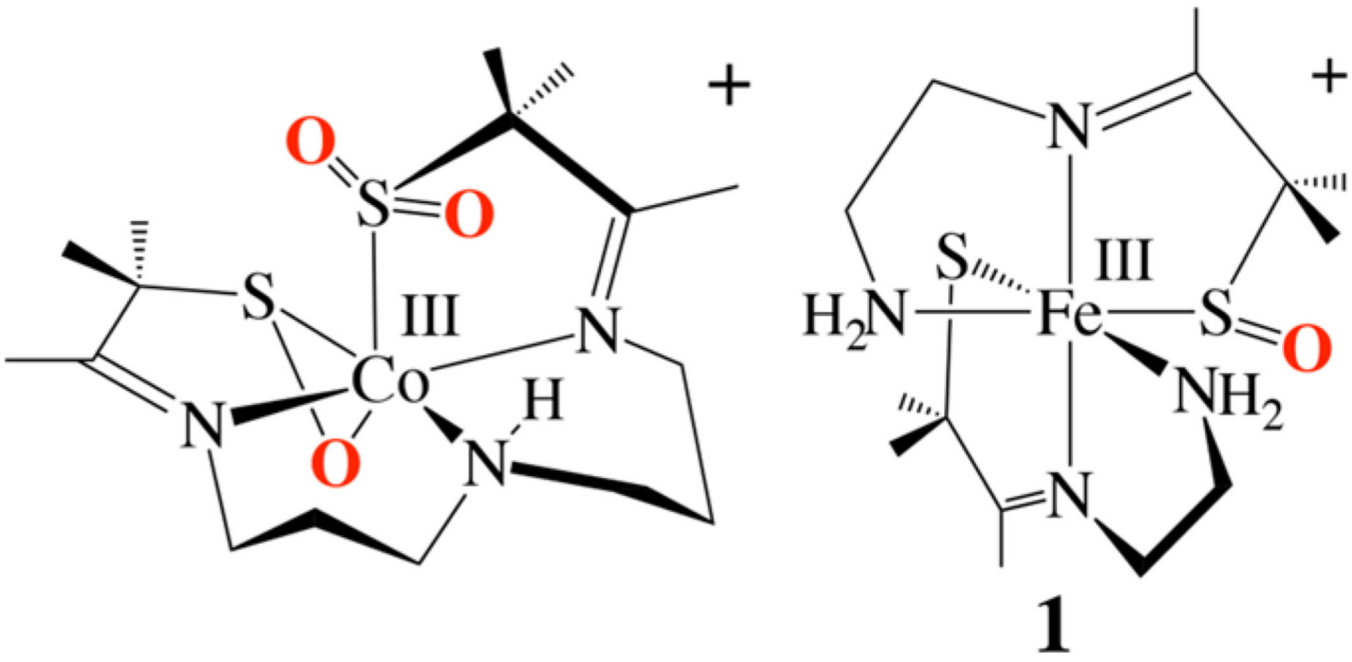

Scheme 2.

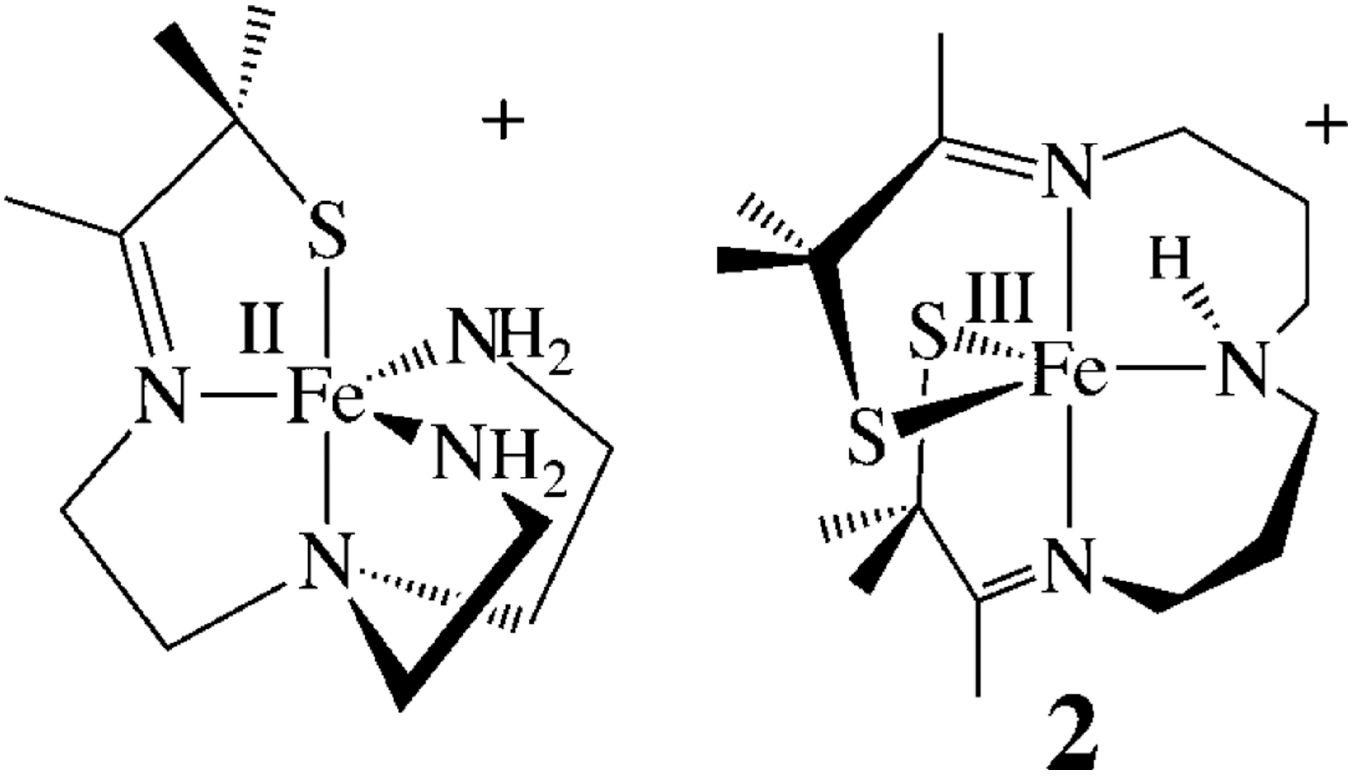

Scheme 3.

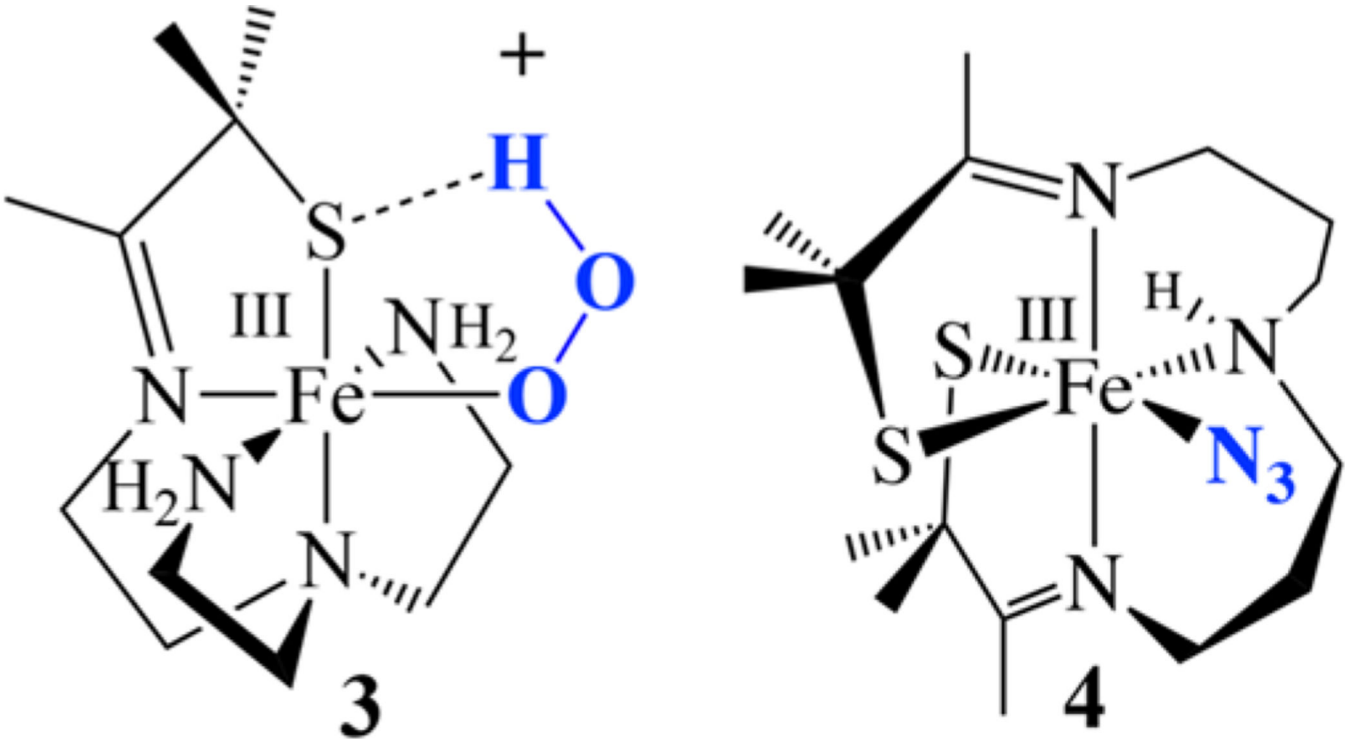

Scheme 4.

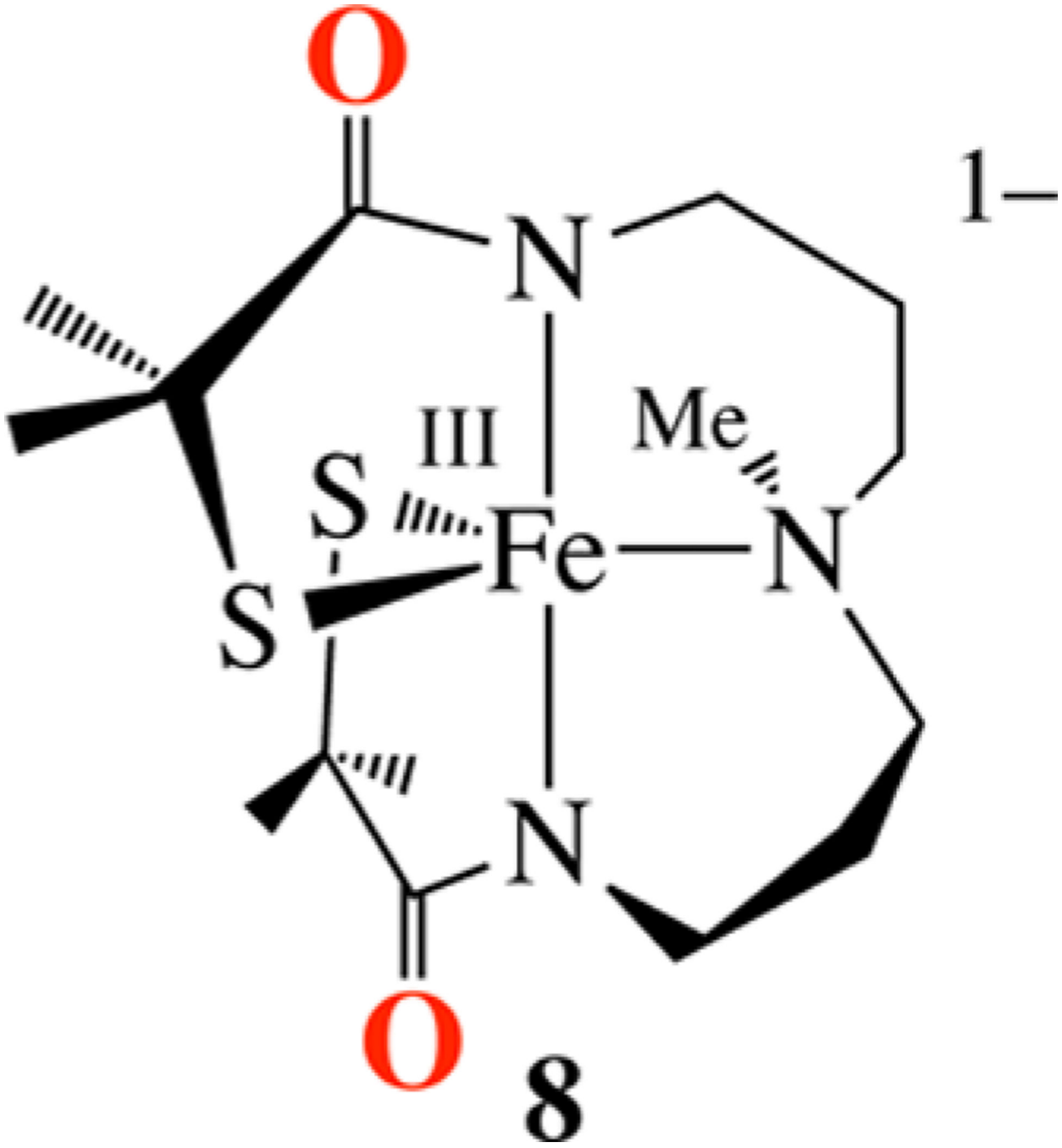

Scheme 5.

Table 1

Crystal Data for [$Fe^{III}(\eta^2\text{-}S^{Me2}O)(S^{Me2}N_3(Pr,Pr)](PF_6)$ (5) and $(Et_4N)[Fe^{III}S_2{}^{Me2}N^{Me}N_2{}^{amide}(Pr,Pr)]$ (8)

	5	**8**
formula	$C_{16}H_{31}F_6FeN_3OPS_2$	$C_{23}H_{47}FeN_4O_2S_2$
MW (g/mol)	546.38	531.62
temp (K)	130(2)	130(2)
unit cell[a]	monoclinic	orthorhombic
space group	*P*21/*c*	*Pna*2$_1$
a (Å)	12.3550(5)	17.9580(3)
b (Å)	15.3070(8)	8.5610(6)
c (Å)	14.8020(7)	18.1560(7)
α (deg)	90	90
β (deg)	123.147(3)	90
γ (deg)	90	90
V (Å^3)	2343.79(19)	2791.3(2)
Z	4	4
σ_{calc} (mg/m^3)	1.548	1.265
R[b]	0.0721	0.0477
R_w	0.2040	0.1219
GOF	1.001	0.940

[a] In all cases: Mo Kα (λ = 0.71070 Å) radiation.

[b] $R = \sum||F_o| - |F_c||/\sum|F_o|$; $R_w = [\sum w(|F_o| - |F_c|)^2/\sum wF_o{}^2]^{1/2}$, where $w^{-1} = [\sigma^2_{count} + (0.05F^2)]/4F^2$.

Table 2

Comparison of Selected Bond Distances (Å) and Angles (deg) for Imine-Ligated $[Fe^{III}(S_2{}^{Me2}N_3(Pr,Pr))]^+$ (2),[63] Its Singly Oxygenated Derivative $[Fe^{III}(\eta^2\text{-}S^{Me2}O)(S^{Me2}N_3(Pr,Pr)]^+$ (5), and Carboxamide-Ligated $[Fe^{III}S_2{}^{Me2}N^{Me}N_2{}^{amide}(Pr,Pr)]^-$ (8)

	2	5	8
Fe–S(1)	2.133(2)	2.142(2)	2.231(1)
Fe–S(2)	2.161(2)	2.148(2)	2.210(1)
Fe–N(1)	1.967(4)	1.976(4)	1.934(3)
Fe–N(2)	2.049(4)	2.044(5)	2.212(3)
Fe–N(3)	1.954(4)	1.954(4)	1.924(3)
Fe–O(1)	N/A	2.115(4)	N/A
S(1)–O(1)	N/A	1.447(6)	N/A
N(1)–Fe–N(3)	178.1(2)	178.0(2)	177.8(1)
S(1)–Fe–S(2)	121.0(1)	112.62(8)	144.40(5
S(1)–Fe–N(2)	132.3(1)	134.1(1)	107.14(9
S(2)–Fe–N(2)	106.5(1)	113.2(2)	108.43(9
S(1)–Fe–N(1)	86.7(1)	86.1(1)	85.37(9)
S(2)–Fe–N(1)	95.2(1)	91.9(1)	93.8(1)
S(1)–Fe–O(1)	N/A	39.7(2)	N/A[a]
O(1)–Fe–S(2)	N/A	152.3(2)	N/A[a]
O(1)–Fe–N(1)	N/A	87.6(2)	N/A[a]
O(1)–Fe–N(2)	N/A	94.3(2)	N/A[a]
O(1)–Fe–N(3)	N/A	94.4(2)	N/A[a]
τ	0.76	N/A	0.56

[a]In this structure, the only oxygens are associated with the carboxamide, and are not coordinated to the metal.